Stochastic Filtering of Rain Profiles using Radar, Surface-Referenced Radar, or Combined Radar/Radiometer Measurements

Ziad S. Haddad
Eastwood 1111
Stephen L. Durden
Scott 1 Iensley

Jet Propulsion laboratory, California Institute of Technology

May 25, 1994

Abstract

We describe a computationally efficient nearly-optimal Bayesian algorithm to estimate rain (and drop-size-distribution) profiles, given a radar reflectivity profile at a single attenuating wavelength. The algorithm also calculates the r.m.s. uncertainty in its estimates. We also describe a more general algorithm that can make estimates based on a radar reflectivity profile together with an approximate measurement of the path-integrated attenuation, or a radar reflectivity profile and a set of passive microwave brightness temperatures.

1 Introduction

It is well-documented (Hitschfeld and Bordan 1954, Meneghini 1978, addad et al 1993) that there are significant ambiguities inherent in the determination of a articular vertical rain intensity profile from a given time profile of radar echo powers measured by a downward looking (spaceborne or airborne) radar at a single attenuating frequency. Indeed, in addition to deriving the formulas that generate all *deterministic* mutually ambiguous rain rate profiles from a given profile of received radar reflectivit its, we have also produced (Haddad et al 1993) a quantitative measure to assess how likely each of these deterministic profiles is, what the appropriate "average>' p rofile should be, and what the "variance" of these multiple solutions is. In order to do this, we formalized the *stochastic* constraints that allow us to make sense of the words "average" and "variance" in a mathematically rigorous way. The quantitative approach we then took to estimate the rain would be particularly well-suited for such systems as the spaceborne Ku-band Precipitation Radar of the Tropical Rainfall Measuring Mission (TRMM), if it were more efficiently implement able in real-time. Indeed, our stochastic approach had so far relied on calculating the full density function for the rain variables conditioned on the radar observations in order to estimate the rain. The resulting algorithm was very cumbersome and computationally intensive. In this work, we present a new extended-Kalman algorithm to calculate the first and second moments of the density function directly. We also extend the approach to account for other observations such as one additional rain-modified surface-reflectivity measurement, or multiple-microwave-frequency radiometer measurements.

2 Mathematical approach

For simplicity, we start with the model that the effective reflectivity $p(r)$, measured at range r by a downward-looking mono-static narrow-band radar such as the TRMM Precipitation Radar, is proportional to the reflectivity coefficient Z of the rain at range r, and to the accumulated attenuation from range 0 (the top of the cloud) to range r. Calling $k(r)$ (resp. $R(r)$) the attenuation coefficient (resp. rain rate) at range r, we assume for simplicity that $Z = aR^b$ and $k = \alpha R^\beta$ for some value of the parameters a, b, α and β, and that the calibrated reflectivity is therefore given by

$$p(r) = aR(r)^b 10^{-0.1(2\int_0^r \alpha R(t)^\beta dt)} \tag{1}$$

Treating a, b, α and β as parameters, the solution to equation (1) can be written as

$$R(r) = \frac{p(r)^{1/b}}{\left(a^{\beta/b} - \frac{0.2\log(10)\alpha\beta}{b}\int_0^r p(t)^{\beta/b}dt\right)^{1/\beta}} \tag{2}$$

Equation (2) suggests that if the rain parameters are not known exactly, mull iple solutions for R can exits. In (Haddad et al 1993), we describe just how mutually ambiguous these multiple solutions can get. In the same paper, we also show that using the surface return as a reference dots not solve the ambiguity problem. Since one has to '(iii\'c with" these ambiguities, it is very important to know how likely each of the multiple solutions is: specifically, given some a-priori "statistical" constraints on the variables involved, one would like to find what the "average" solution to (2). Using average values for the rain parameters is still not sufficient because even when exact values for o, b, α and β are given, it is known that the numerical implementation of equation (2) gives a numerically *unstable* "inversion" algorithm.

Thus one is naturally led to a stochastic filtering approach. One would like to introduce a "measure" on the set of all ambiguous profiles giving rise to the same measured reflectivity profile, and try to find the "average" profile with respect to this measure on this set, along with an estimate of the mean difference between the members of this set of mutually ambiguous profiles. In (Haddad et al, 1993), we described an algorithm to compute the joint probability density function 'P for $\{R(r)$, o, $b, \alpha, \beta\}$ given measurements of $p(r)$. The "average" rain profile and the "mean deviation" with all the mutually ambiguous profiles can then be obtained from the moments of $\mathcal{P}$. Indeed, the results reported in (Haddad et al, 1 993) have been very encouraging. In particular, in the case where o, b, α and β are assumed known, *this approach yields a stable inversion algorithm which does not require any surface reference information.* But calculating the full density function requires large amounts of co nputer m emory and CPU time, too large to make the algorithm useful in anywhere near real-time. In order to reduce the amount of computer resources required, rather than calculating $\mathcal{P}$ itself, one can try to compute its mean and covariance directly. This amounts to deriving the extended Kalman filter appropriate to the p roblem at hand. We now describe how this is done.

First, we need to specify the a-priori constraints 011 the "state variables" $R(r)$, a, b, α, β and $c(r) = \int_0^r \alpha R^\beta$. For simplicity, we shall assume that a, b, α and β are constant, that the only constraint on c is that it be the integral with respect to r of $\alpha R(r)^\beta$, and we express the requirement that R itself be positive and continuous by writing

$$R(r) = e^{x(r)+\lambda r} \tag{3}$$

where x is the (mathematically) simplest continuous stochastic process and λ a suitable factor (possibly zero) to be determined. Specifically, without further a-priori information,

we assume that $x(r) = x(0) + \sigma b(r)$, where $x(0)$ and $b(r)$ are independent, $x(0)$ itself is Gaussian with mean m_0 and variance σ_0^2, and the process $b(r)$ has independent 0-mean Gaussian increments with variance equal to the extent in range of the increment interval. Thus, in effect, we are assuming that the a-priori constraints on the evolution of $\log(R)$ with range r are those of standard Brownian motion, up to a possible "drift" term λr.

Now that we have established the a-priori constraints on the dynamics of our variables, we must make explicit the function $h(r)$ expressing our measurement from range r in terms of our state variables. From equation (1), one can see that

$$h(r) = \log(a) + b(x(r) + \lambda r) - 0.2\log(10)c(r) + \text{Noise.} \tag{4}$$

Let us write σ_N for the r. m.s. noise level in the measurements, which, for simplicity, we shall attribute here to Rayleigh fading only (system noise can be aken into account, at the expense of making the exposition somewhat more cumbersome). Since our data consist of the averaged power of M independent pulses, tile noise term in (4) would be the logarithm of the average of the squared-magnitudes of M independent standard complex Gaussian variables. Hence, as soon as $M > 4$, it is quite reasonable to assume that this noise term is itself approximately a 0-mean normal variable with variance $\sigma_N^2 \simeq 1/M$.

We are now ready to apply the standard machinery of stochastic filtering to obtain the best estimate $\hat{R}(r)$ of tile rain rate at range r given all the observations. Since the relation $dc/dr = \alpha R^\beta$ is non-linear, we cannot use a straightforward Kalman filter to solve the problem. We chose to use an extended Kal man filter approach, using a first-order Taylor series linearization to obtain both the downward estimate (starting from the top of the cloud $r = 0$) and the upward estimate (starting from the ocean surface). The theory and details behind the technique can be found for example in Øksendal, 1985, or Jazwinski, 1970. For completeness, we summarize the flow of the particular algorithm in the case at hand, when the parameters a, b, α and β are assumed known.

First, one must obtain "downward" estimates $\hat{x}_d(r)$ and $\hat{c}_d(r)$ of the state variables x and c at all ranges r based on all earlier measurements obtained for $r' < r$, along with their covariances $p_{xx}(r)$, $p_{cx}(r)$ and $p_{cc}(r)$. To do this, one must start with

$$\hat{x}_d(0) = m_0 \tag{5}$$
$$\hat{c}_d(0) = 0 \tag{6}$$
$$p_{cc}(0) = 0 \tag{7}$$
$$p_{cx}(0) = 0 \tag{8}$$
$$p_{xx}(0) = \sigma_0^2. \tag{9}$$

Then, given our estimates at range r, the estimates at range $r + \delta$ can be obtained in two

steps, by first accounting for the changes in the dynamics using the formulas

$$\tilde{x}(r+\delta) = \hat{x}_d(r) \tag{10}$$

$$\tilde{c}(r+\delta) = \hat{c}_d(r) + \alpha \int_r^{r+\delta} e^{\beta(\tilde{x}(t)+\lambda t)} dt \tag{11}$$

$$\tilde{p}_{xx}(r+\delta) = p_{xx}(r) + \sigma^2 \delta \tag{12}$$

$$\tilde{p}_{cx}(r+\delta) = p_{cx}(r) + \alpha\beta \int_r^{r+\delta} e^{\beta(\tilde{x}(t)+\lambda t)} \tilde{p}_{xx}(t) dt \tag{13}$$

$$\tilde{p}_{cc}(r+\delta) = p_{cc}(r) + 2\alpha\beta \int_r^{r+\delta} e^{\beta(\tilde{x}(t)+\lambda t)} \tilde{p}_{cx}(t) dt, \tag{14}$$

then by accounting for the measurement $z(r+\delta)$ obtained from range $r+\delta$ using the formulas

$$\hat{x}_d(r+\delta) = \tilde{x}(r+\delta) + \frac{b\tilde{p}_{xx}(r+\delta) - 0.2\log(10)\tilde{p}_{cx}(r+\delta)}{D}\Delta \tag{15}$$

$$\hat{c}_d(r+\delta) = \tilde{c}(r+\delta) + \frac{b\tilde{p}_{cx}(r+\delta) - 0.2\log(10)\tilde{p}_{cc}(r+\delta)}{D}\Delta \tag{16}$$

where $D = (0.2\log(10))^2\tilde{p}_{cc}(r+\delta) - 2(0.2\log(10))b\tilde{p}_{cx}(r+\delta) + b^2\tilde{p}_{xx}(r+\delta) + \sigma_N^2$, and $\Delta = z(r+\delta) - (\log(a) + b(\tilde{x}(r+\delta) + \lambda r) - 0.2\log(10)\tilde{c}(r+\delta))$ measure the amount by which the observation that would correspond to the preliminary estimates $\tilde{x}$ and $\tilde{c}$ differs from the actual measurement.

The upward portion of the algorithm, to obtain "upward" estimates $\hat{x}_u(r)$ and $\hat{c}_u(r)$ of the state variables x and c at all ranges r based on all further measurements obtained for $r' > r$, proceeds in a similar fashion, except for the obvious sign changes that are then necessary. One must then combine downward and upward estimates to obtain the optimal estimates $\hat{x}$ and $\hat{c}$ based 011 **all** the reflectivity data. This is done using the formula

$$\begin{pmatrix} \hat{c} \\ \hat{x} \end{pmatrix} = \left(P_d^{-1} + P_u^{-1}\right)^{-1} \left(P_d^{-1} \begin{pmatrix} \hat{c}_d \\ \hat{x}_d \end{pmatrix} + P_u^{-1} \begin{pmatrix} \hat{c}_u \\ \hat{x}_u \end{pmatrix}\right) \tag{17}$$

at every range r, with P denoting the appropriate covariance IIlat7'ices (we have tacitly assumed that all variables are evaluated at the same range r). The optimal estimate $\hat{R}_{radar}(r)$ of the rain rate itself is then given by the mean $\mathcal{E}e^{x(r)+\lambda r}$, which, since x itself is Brownian, becomes

$$\hat{R}_{radar}(r) = e^{\hat{x}(r)+0.5p_{xx}(r)+\lambda r} \tag{18}$$

and its r.m.s. uncertainty $\sigma_{radar}(r)$ by

$$\sigma_{radar}(r) = \hat{R}_{radar}(r) \cdot \sqrt{e^{p_{xx}(r)} - 1} \tag{19}$$

As expected, the resulting algorithm turns out to be orders of magnitude more efficient than the full density function approach described in (Haddad et al, 1993). Before discussing the practical applications, we still need to describe how one specifies values for the parameters m_0, σ_0, σ and λ. Although, as we shall see, in practice, the exact values do not affect the estimation algorithm significantly (after all, when a, b, α and β are known, the theoretical solution is unique), one should certainly try to give them at least physically reasonable values. '1'0 do that, we use the a-priori constraints which we have imposed. It follows from (3) that the expected value of the *ail)-rate $R(0)$ at the top of the rain column is

$$\mathcal{E}\{R(0)\} = e^{m_0 + \frac{1}{2}\sigma_0^2} \tag{20}$$

and its relative variance is

$$\mathcal{E}\left\{\left(\frac{R(0)}{\mathcal{E}\{R(0)\}} - 1\right)^2\right\} = \frac{\mathcal{E}\{R(0)^2\}}{\mathcal{E}\{R(0)\}^2} - 1 = e^{\sigma_0^2} - 1 \tag{21}$$

In practice, we set a minimum "threshold onset" value R_{min} for the smallest significant rain rate we expect at the top of the rain column, along with some estimate for the associated mean relative uncertainty. Equation (21) then implies that we should choose

$$\sigma_0^2 = \log\left(\frac{\mathcal{E}\{R(0)^2\}}{R_{min}^2}\right) \tag{22}$$

and (20) in turn implies that we should then choose

$$m_0 = \log(R_{min}) - \frac{1}{2}\sigma_0^2 \tag{23}$$

The choice of λ is somewhat more problematic. We do know that, a priori, by definition, the rain rate should initially increase with range from the a-priori value R_{min}. This would imply a positive drift λ. '1'0 get a value for λ, we look at the terminal behavior of R. Writing $R'(r)$ for $R'(r) = R(r_s - r)$, where r_s is the range of the surface, and if we reverse the constraint (3) in time to apply it to $R'(r)$, one finds that the "a-priori" (with time reversed) expected value for R' will be given by

$$\mathcal{E}\{R'(r)\} = e^{\hat{r}_d(r_s) + \frac{1}{2}p_{xx}(r_s) + \lambda r_s} \cdot e^{(\frac{1}{2}\sigma^2 - \lambda)r} \tag{24}$$

Since we have a priori no reason to expect the rain rate to increase or decrease as one moves up from the bottom of the rain column, it is natural to choose the value

$$\lambda = \frac{1}{2}\sigma^2 \tag{25}$$

Last, we must decide on a value for σ. In practice, this parameter controls the a priori variation $\mathcal{E}\{(x(r+\delta) - x(r))^2\} = \sigma^2\delta$. In fact, the average a priori rate-of-change of R is given by

$$\mathcal{E}\left\{\frac{R(r+\delta)}{R(r)}\right\} = e^{\sigma^2\delta} = \frac{\mathcal{E}\{R(r+\delta)\}}{\mathcal{E}\{R(r)\}} \tag{26}$$

We therefore choose an a priori value for $\mathcal{E}\{R(r+\delta)/R(r)\}$ and use (26) to deduce the corresponding value of σ.

3 Applications – radar only

In practice, we started with the values $a = 255$, $b = .31$, and the typical Ku-band values $\alpha = 0.0285$ and $\beta = 1.1$. To determine the parameters σ_0 and m_0, we use equations (22) and (23), except that rather than specifying R_{min} and its variance directly, we specify the minimum threshold-onset reflectivity Z_{min} and its variance. Practically, we set $10\log_{10}(Z_{min}) = 26$ dB, so that nominally $R_{min} = (Z_{min}/a)^{1/b} \simeq 1.4$ mm/hr in our case, then we used this value in (23), with the following values in equation (22): $\sigma_0^2 = \log(10^{(0.1)\cdot(2.3)})$. Finally, for σ, we used the value given by equation (26) with $\mathcal{E}\{R(r+1)/R(r)\} = 1.5$, r in km.

To test our algorithm, we then synthesized radar reflectivity profiles starting with each of three assumed rain rate profiles, using fading noise corresponding to the average of 50 independent pulses. The three input rain rate profiles were

Profile A (linear-then-constant): the rain increases linearly from 1 mm/hr at range O up to 5 mm/hr at range $r = 2$ km, then remains constant at 5 mm/hr until the surface range $r_s = 5$ km (see figure 1).

Profile B (sawtooth-linear): the rain increases linearly from 1 mm/hr at range O up to 25 mm/hr at range $r = 2$ km, then decreases linearly down to 12.5 mm/hr at range $r = 3$ km, then back up to 25 mm/hr at $r = 4$ km, and finally back down to 12.5 km at $r_s = 5$ km (see figure 2a).

Profile C (sawtooth-linear): the rain increases linearly from 1 mm/hr at range O up to 75 mm/hr at range $r = 2$ km, then decreases linearly down to 37.5 mm/hr at range $r = 3$ km, then back up to 75 mm/hr at $r = 4$ km, and finally back down to 37.5 km at $r_s = 5$ km (see figures 3a and 3b).

We then supplied the synthesized reflectivity profiles as input to our algorithm to estimate the associated rain rates. Figure 1 shows the estimated rain rate profile and the associated r.m.s. uncertainty when the input was profile A. The estimates are manifestly quite accurate.

We tried changing the value of Z_{min} over the interval $20 \leq Z_{min} \leq 32$ dB, with results that were less than 1% off the ones in figure 1. Figure 2a shows the estimates of our algorithm when the input profile was profile B. Figure 2b shows the estimates when $\mathcal{E}\{R(r+1)/R(r)\}$ is increased up to 3, and figure 2c shows the estimates when $\mathcal{E}\{R(r+1)/R(r)\}$ is given the value 1.1 the effects are smaller than the r.m.s. uncertainty in the estimates. Figures 3a and 3b show what can happen at larger rain rates, specifically when the input is profile C. The estimates in both cases are quite close to the actual values up to a range of 3 km. Beyond that, the algorithm begins to over- or under-estimate noticeably. The reason for the discrepancy is that the intrinsic ambiguities in the rain-rate reflectivity-profile relation can be quite pronounced, especially at higher rain rates. In fact, in general, by changing the rain parameters a, b, α or β by small amounts, one can succeed in constructing substantially different rain profiles that produce identical reflectivity profiles. As was shown in (Haddad et al, 1993), at high rain rates, the exponential contribution of these ambiguitites can grow very quickly. Figure 3a shows our algorithm's estimates with the original parameter values as above, and figure 3b shows the estimates when b is changed from 1.31 to 1.313, i.e. by a mere 0.2% ! The ambiguity is responsible for the increasing r.m.s. uncertainty in the estimates: the algorithm recognizes that its estimates are less and less precise as the potential for ambiguity increases with range. One conclusion that can be drawn from these observations is that it would be obviously unwise in practice to fix values for the rain parameters a, b, α and β, especially in cases where one expects sustained high rain rates. Instead, one should modify the model to allow these parameters to be themselves stochastic, as was done in our previous full-density-function approach (Haddad et al, 1993). now this can be done while still keeping the algorithm efficient is described in the next section.

We end our radar-only test cases with measured data. Figure 4a shows the estimated rain rate obtained using our extended-Kalman algorithm with the original parameter values, when the input was one of the radar reflectivity profiles measured by JPL's ARMAR radar (Durden et al, 1992) over the Western Pacific Ocean during the TOGA-COARE experiment on February 4, 1993, at 15:35 local time. Details of the participation of ARMAR in COARE can be found in (Li et al, 1993). Figure 4b shows our algorithm's estimates when the rain parameter values were changed to $a = 300$, $b = 1.4$, $\alpha = 0.026$, $\beta = 1.08$. The relative difference in the estimates increases, especially over the last two kilometers where it goes from 100 % up to close to 300 %. For comparison, figure 4c shows the estimates obtained using our full-density-function code (from Haddad et al, 1993), where we had again assumed that $a = 300$, $b = 1.4$, $\alpha = 0.026$, $\beta = 1.08$, The difference between the two model's in the stochastic constraints on the rain rate explain the difference in the r.m.s. uncertainty values between the two graphs. Otherwise, the estimates are remarkably close. Yet while the results of our old full-density-function algorithm took several hours of computer CPU time to produce, the estimates of the extended-Kalman algorithm took less than a second.

We shall return to the ARMAR data in the last section in order to illustrate how radiometer measurements can help determine the correct parameter values to use, and reduce the uncertainty in the estimates.

4 Coupled DSD-based Z–R and k--it relations

Rather than use the independent power-law Z- R and k- R relations above, and allow the parameters a, b, α and β to vary independently, we will use more realistic *coupled* relations, based on the drop size distribution (DSD). Specifically, following Ulbrich, 1983, we shall assume

- that the DSD at range r is given by $N(D;r) = N_0(r)D^{\mu}e^{-\Lambda(r)D}$, for all $D > 0$, with $-1 < \mu$,
- that N_0 is related to the rain rate R by $N_0(r) \simeq 140R(r)\Lambda(r)^{4.67+\mu}/\Gamma(4.67+\mu)$, when D is expressed in mm, R in mm /hr, and $N(D)dD$ in number of drops per m^3 this follows directly from the assumption that all drops are falling at their power-law terminal velocity (see Haddad et al, 1993, for details),
- that the mass-weighted mean drop diameter, $(\mu+4)/\Lambda(r)$, is related to the rain-rate by a power-law $(\mu+4)/\Lambda(r) = R(r)^{\delta}$, where the parameter δ can vary over the interval $0.08 \leq \delta \leq 0.23$ (again, see Haddad et al, 1994, for the details),
- that μ, δ and R are a priori independent,
- and that μ and δ are (for now) constant over the rain column.

Thus we are describing the rain column by specifying the DSD at every range R, using the rain rate profile $R(r)$ and two additional parameters, μ and δ. As stated above, we shall start by assuming that these two additional parameters are constant over the rain column. As we shall see later, this simplifying assumption is not crucial to the derivation of the algorithm. Using this description of the rain, one can replace the power-law Z- R and k- R relations by any more realistic physical model such as Mie-scattering or a T-matrix calculation. For this paper, however, we shall stay with the simple power-law models. Under the Rayleigh hypothesis (for Z), and using a power law to relate the total scattering cross-section of a drop to its diameter (for k), the above assumptions produce the relations

$$Z = 140\frac{\Gamma(7.26+\mu)}{\Gamma(4.67+\mu)\cdot(4+\mu)^{2.59}}R^{1+2.59\delta} \tag{27}$$

$$\text{and} \quad k = 0.026\frac{\Gamma(5.33+\mu)}{\Gamma(4.67+\mu)\cdot(4+\mu)^{0.86}}R^{1+0.86\delta} \tag{28}$$

One can readily verify from these equations that the values $(a, b, \alpha, \beta) = (255, 1.31, 0.0285, 1.1)$ used above correspond to $\mu \simeq 1.5$, $\delta \simeq 0.12$, values that are well within the range of both parameters.

5 Incorporating additional measurements

The previous sections described how to estimate the rain variables given the radar reflectivities only. While that is interesting in itself, one would like to be able to account for additional measurements, such as passive microwave brightness temperatures, to reduce the inherent ambiguity. The Bayesian approach which we have taken so far can guide us in performing this data fusion. Indeed, calling $\vec{T}$ the vector of brightness temperatures, we need to compute the conditional density function $\mathcal{P}(\{R(r)\}_{0\le r\le r_s}, \mu, \delta | \vec{T}, p(r))$ for the rain variables $\{R(r)\}_{0\le r\le r_s}$, μ and δ, given a reflectivity profile $p(r)$ and a set of brightness temperatures $\vec{T}$. By Bayes's theorem, this probability is given by

$$\mathcal{P}(\{R(r)\}_{0\le r\le r_s}, \mu, \delta | \vec{T}, p(r)) = \mathcal{P}(\vec{T} | \{R(r)\}_{0\le r\le r_s}, \mu, \delta, p(r)) \cdot \mathcal{P}(\{R(r)\}_{0\le r\le r_s}, \mu, \delta | p(r)) \cdot K_0 \tag{29}$$

where K_0 is the over-all normalization constant making the integral of the left-hand-side equal to 1. Let us now examine (29) carefully.

The first term in the right-hand-side of (29) is the probability of the brightness temperatures $\vec{T} = (T_1, \ldots, T_j, \ldots)$ given all the other data. This figure can be obtained using a "forward" model to compute the brightness temperature from the physical rain data. In fact, we shall assume that we have an efficient deterministic forward algorithm to compute the "mean" brightness temperatures $\hat{T}_j$ at the relevant frequencies that correspond to a given rain profile, along with an approximate formula giving the r.m.s. deviation $\sigma_{\hat{T}_j}$ to be expected about each **of** these average brightness temperatures. Given such a forward model, we can replace the first probability in the right-hand-side Of (29) by the product of Gaussians $\mathcal{G}_{\sigma_{\hat{T}_j}}(T_j - \hat{T}_j)$ with mean $\hat{T}_j$ and variance $\sigma^2_{\hat{T}_j}$. Thus,

$$\mathcal{P}(\vec{T} | \{R(r)\}_{0\le r\le r_s}, \mu, \delta, p(r)) \simeq \prod_j \mathcal{G}_{\sigma_{\hat{T}_j}(\mu,\delta,p(r))}\left(T_j - \hat{T}_j(\mu, \delta, p(r))\right) \tag{30}$$

where we have made explicit the dependence of $\hat{T}_j$ and $\sigma_{\hat{T}_j}$ on the rain data $(\mu, \delta, p(r))$.

The second term in the right-hand-side of (29) can be further split into the product of two simpler terms, thanks again to Bayes's theorem:

$$\mathcal{P}(\{R(r)\}_{0\le r\le r_s}, \mu, \delta \mid p(r)) = \mathcal{P}(\{R(r)\}_{0\le r\le r_s} \mid \mu, \delta, p(r)) \cdot \mathcal{P}(\mu, \delta | p(r)) \cdot K_1 \tag{31}$$

In the right-hand-side of (31), the first term is exactly what our extended Kalman filter described in the earlier sections computes: the probability function for the rain rate profile, assuming μ and δ and the radar reflectivities are known. More precisely, our extended-Kalman-filtering algorithm computes the first two moments of this density function. The second term in the right-hand-side is the density function of μ and δ given the radar reflectivities. We shall approximate it with the a priori density function $\mathcal{P}(\mu, \delta)$ for μ and δ, namely a product of two independent uniform distributions. Last, the normalization constant K_1 must take on that value which makes the left-hand-side integrate to 1.

Putting (29), (30) and (31) together, one thus finds that

$$\mathcal{P}(\{R(r)\}_{0\le r\le r_s}, \mu, \delta | \vec{T}, p(r)) \simeq \mathcal{P}(\{R(r)\}_{0\le r\le r_s} | \mu, \delta, p(r)) \cdot \mathcal{P}(\mu, \delta) \cdot K \cdot \prod_j \mathcal{G}_{\sigma_{\hat{T}_j}} \left(T_j - \hat{T}_j(\mu, \delta, p(r)) \right) \tag{32}$$

where the first moments of the first term on the right are computed by the extended-Kalman-filter described in the previous sections, and where K represents the normalization constant $K_0 \cdot K_1$. We are finally ready to write down explicit expressions for the optimal estimates of μ, δ and $R(r)$ given $p(r)$ *and* $\vec{T}$. Indeed, all we need to do is calculate the various means of (32). Thus, the optimal estimate $\hat{R}_{radar+passive}(r_0)$ for $R(r_0)$ at any range r_0 is obtained by taking the mean of $R(r_0)$:

$$\begin{aligned} \hat{R}_{radar+passive}(r_0) &= \int R(r_0) \cdot \mathcal{P}\left(\{R(r)\}_{0\le r\le r_s}, \mu, \delta \mid \vec{T}, p(r) \right) \, d\{R(r)\} d\mu d\delta \qquad (33) \\ &\simeq K \cdot \int\int \hat{R}_{radar}(r_0; \mu, \delta) \cdot \mathcal{P}(\mu, \delta) \cdot \left(\prod_j \mathcal{G}_{\sigma_{\hat{T}_j}(\mu,\delta,p(r))} \left(T_j - \hat{T}_j(\mu, \delta, p(r)) \right) \right) \, d\mu d\delta \end{aligned}$$

where $\hat{R}_{radar}(r_0; \mu, \delta)$ is the radar-only estimate obtained as in formula (1 S). Thus, the optimal estimation of the rain rate proceeds in two steps: first, we compute the radar-only estimates using an efficient extended-Kalman-filtering approach, for each possible pair (μ, δ); next, again for each (μ, δ), we calculate the corresponding brightness temperatures. Finally, at each range r_0, we perform the double integration specified in (33) to estimate the rain rate itself at that range.

If, instead of passive microwave brightness temperatures, our additional measurement consisted of the path-integrated attenuation (PIA), we would use a similar algorithm to improve our radar-only estimates and condition them further on this additional measurement. Indeed, in this case, the optimal estimate would be

$$\hat{R}_{radar+PIA}(r_0) \simeq K' \cdot \int\int \hat{R}_{radar}(r_0; \mu, \delta) \cdot \mathcal{P}(\mu, \delta) \cdot \mathcal{G}_{\sigma_{\hat{c}}} (C - \hat{c}(r_s; \mu, \delta)) \, d\mu d\delta \qquad (34)$$

where C is the measured PIA, $\hat{c}(r_s; \mu, \delta)$ the path-integrated attenuation from the top of the rain column to the surface range r_s as estimated by the extended Kalman algorithm, for each (μ, δ), and $\sigma_{\hat{c}}$ the associated standard deviation.

The estimates (33) and (34) can be compared with the radar-only estimate

$$\hat{R}_{radar}(r_0) \simeq K'' \cdot \int\int \hat{R}_{radar}(r_0;\mu,\delta) \cdot \mathcal{P}(\mu,\delta)\, d\mu d\delta. \tag{35}$$

Similarly, in each of these three cases (racial-olllly, radar+ passive, radar+ I'IA), one can compare the variance of $\hat{R}$, i.e. the error bar that the algorithm itself imposes on its own estimate, in order to decide how the ambiguity is being reduced, if at all.

6 Applications

Figure 5 shows the graph of the "forward" function we used o compute the average 13.8 GHz brightness temperature $\hat{T}_j(\mu, \delta, p(r))$, namely

$$\hat{T}_j(\mu, \delta, p(r)) = T' + \epsilon(t - T')10^{-0.1\hat{c}(r_s)} - T'(1 - \epsilon)10^{-0.2\hat{c}(r_s)} \tag{36}$$

where ϵ = the surface emissivity $\simeq$ 0,3S, T' = the atmosphere (physical) temperature $\simeq$ 280'' 1(, t = the surface (physical) temperature $\simeq 300°K$, and where $\hat{c}(r_s)$ is the estimated integrated attenuation at the surface $r = r_s$, which is computed by our extended-Kalman algorithm as a function of μ, δ and the input profile $p(r)$. For every value of ϵ, earlier calculations (Durden et al, 1 994) have quantified the expected spread of the associated brightness temperatures: the minimum and maximum values are shown by the dotted curves in figure 5. We added this inherent variance in the forward formula to the variance due to the uncertainty $\sigma_{\hat{c}}$ in our estimate of $\hat{c}(r_s)$ **to** obtain an approximation to the m.s. deviation $\sigma_{\hat{T}_j}$ of the brightness temperature predicted by (36).

Starting with independent uniform distributions for μ over the interval [- 0.5, + 3.5] and for δ over [0.08, 0.23], we then used formulas (35), (34) and (33) to obtain radar-only, radar+PIA and racial+-racliolllctcl' estimates for each of our sample profiles considered in section 3. Figure 6a shows the result of the radar-only estimation (35) in the case of profile B. Figure 6b shows the result of the radar+ PIA estimation (refsixteen) assuming that the path-integrated attenuation is the one corresponding to profile B, namely 0.695 d]], up to an r.m.s. uncertainty of 0.1 dB, and figure 6c shows the estimate when the PIA uncertainty is assumed to be 0.5 dB. The uncertainty in the resulting rain-rate estimates decreases then increases accordingly. Figure 6d shows the radar-1 radiometer estimates using (33), where the passive microwave brightness temperatures are handled as described in the previous paragraph. In this case, figure 5 implies that the uncertainty in the relation between the brightness temperature $T_b \simeq 242.5°K$ and the radar attenuation is relatively small. The accuracy of the radar+ radiometer estimates is therefore quite good, and their uncertainty

quite small. Figures 7abcd show what happens at higher rain rates. Figure 7a shows the radar-only estimates in the case of profile C. The r.m.s. uncertainty in the estimates exceeds 50% at ranges above 1.5 km, as could have been expected from the ambiguity calculations in (Haddad et al, 1993). Figure 7b shows the improved result when one uses the radar+PIA estimates assuming that the path-integrated attenuation is the one corresponding to profile C, namely 3.13 dB, up to an r.m.s. uncertainty of 0.1 dB again. Figure 7c shows the estimates when the PIA uncertainty is assumed to be 0.5 dB. The uncertainty in the resulting rain-rate estimates increases slightly, but remains far smaller than that of the radar-only estimates. In fact, even at the surface range where it is largest, the r.m.s. uncertainty amounts to a reasonable 30%. Figure 7d shows the radar+radiometer estimates. In this case, figure 5 shows that the uncertainty in the relation between the brightness temperature $T_b \simeq 279° K$ and the radar attenuation is quite large. The accuracy of the radar+radiometer estimates at ranges beyond about 3 km is therefore quite unsatisfactory, and their r.m.s. uncertainty is correspondingly large.

Finally, we return to the case where our radar reflectivity profile is the ARMAR TOGA-COARE profile of figures 4abc. Figure 8a shows our radar-only algorithm's estimates. Their associated uncertainty is unacceptably high. Figure 8b shows the radar+PIA estimates, assuming that the path-integrated attenuation is the one estimated by comparing the surface return with the "clear-air surface return" as explained in (Durden et al, 1994), namely 3.9 dB, up to a postulated r.m.s. uncertainty of 0.5 dB. It is most interesting to compare this estimated profile to the one in figure 8c, obtained using the radar+radiometer algorithm with the measured brightness temperature $T_b = 254.3° K$. Since the calibration of ARMAR's passive microwave measurements is not quite complete, we have computed the estimated profiles corresponding to $T_b = 250° K$ (figure 8e), and $T_b = 260° K$ (figure 8d). As the measured microwave temperature decreases or increases, the estimated profile follows suit appropriately.

Future work will concentrate on

- making the forward passive microwave calculation more realistic,
- incorporating additional passive microwave channels,
- modeling the full covariance between μ, δ and R in order to reduce the ambiguities in the radar-only model,
- and increasing the number of variables to allow μ and δ (and hence the drop size distribution) itself) to vary as a function of range.

7 Acknowledgements

This work was performed at the Jet Propulsion Laboratory, California Institute of Technology, under contract with the National Aeronautics and Space Administration.

8 References

Durden, SL, Tanner, A, Wilson, W', Li, 1'', and Ricketts, W: "The NASA/JPL Airborne Rain Mapping Radar (ARMAR)", in Proc. 11th Intl. Conf. Clouds and Precip. 1992,])]). IOI3-1OI6.

Durden, SL, Haddad, ZS, Im, E, Li, FK, Tanner, AB, and Wilson, WJ: "Measurement of rainfall path integrated attenuation at nadir: a comparison of radar and radiometer methods at 13.8 GHz", submitted to *Radio Sci.* (1994).

Hitschfeld, W, and Bordan, J: "Errors inherent in the radar measurement of rainfall at attenuating wavelengths", *J. Meteor.* 11 (1954): pp. 5s-67.

Haddad, ZS, Im, E, and Durden, S: "Estimation of rain rate profiles from radar returns at attenuating wavelengths", in Proc. 26th Intl. Conf. Radar Meteo. 1993, pp. 699-701 .

Haddad, ZS, Im, E, and Durden, S: "Intrinsic ambiguities in the retrieval of rain rates from radar returns at attenuating wavelengths", submitted to *J. App. Meteo.* (1993).

Haddad, ZS, Jameson, AR, Im, E, and Durden, S: "Improved coupled Z R and k-R relations and the resulting ambiguities in the determination of the vertical distribution of rain from the radar backscatter and the integrated attenuation", submitted to *J. App. Meteo.* (1994).

Jazwinski, All: *Stochastic processes and filtering theory*, Academic Press, San Diego, 1970.

Li, F, Durden, SL, Im, E, Tanner, A, Wilson, W, and Ricketts, W: "Airborne Rain Mapping Radar and preliminary observations during TOGA-COARE", in Preprints IGARSS '93,])]). 835-837.

Meneghini, R: "Rain rate estimates for an attenuating radar", *Radio Science* 13 (1978): pp. 459-470.

Oksendal, B: *Stochastic differential equations*, Springer-Verlag, Berlin, 1985.

Ulbrich, CW: "Natural variations in the analyt ical form of the raindrop size distribution", *J. A ppl. Meteo.* 22 (1983): pp. 1764-1775.

Figure captions

Figure 1: Radar-only rain estimates for profile A, assuming a 255, b = 1.31, α 0.02s5. β = 1.1

Figure 2a: Radar-only rain estimates for profile B, assuming a 255, b = 1.31, α 0.02s5, β = 1.1, and $\mathcal{E}\{R(r+1)/R(r)\}$ = 1.5

Figure 2b: Same as 2a, except $\mathcal{E}\{R(r+1)/R(r)\}$ = 3

Figure 2c: Same as 2a, except $\mathcal{E}\{R(r+1)/R(r)\}$ = 1.1

Figure 3a: Radar-only rain estimates for profile C, assuming a 255, b = 1.31, α 0.0285, β = 1.1

Figure 3b: Same as 3a, except b = 1.313

Figure 4a: Radar-only rain estimates for an ARMAR profile measured during TOGA COARE, assuming a = 255, b = 1.31, α = 0.0285, β = 1.1

Figure 4c: Full-density function estimates assuming a = 300, b = 1.4, 0 = 0.026, β = 1.08

Figure 5: Simplified PIA-T_b relation

Figure 6a: Radar-only rain estimates for profile B, assuming $-0.5 < \mu \leq 3.5$ and $0.08 < \delta \leq 0.23$

Figure 6b: Radar+PIA rain estimates for profile B, assuming PIA = 3.13 ± 0.1 dB

Figure 6c: Radar+PIA rain estimates for profile B, assuming PIA = 3.1340.5 dB

Figure 6d: Radar+ radiometer rain estimates for profile B, assuming $T_b = 242.5°K$

Figure 7a: Radar-only rain estimates for profile C, assuming $-0.5 < \mu \leq 3.5$ and $0.08 < 6 < 0.23$

Figure 7b: Radar+PIA rain estimates for profile C, assuming PIA = 10.43- 0.1 dB

Figure 7c: Radar+PIA rain estimates for profile C, assuming PIA = 10.4 ± 0.5 dB

Figure 7d: Radar+ radiometer rain estimates for profile C, assuming $T_b = 279°K$

Figure 8a: Radar-only rain estimates ARMAR / TOGA-COARE profile, assuming $-0.5 \leq \mu \leq 3.5$ and $0.08 \leq \delta \leq 0.23$

Figure 8b: Radar+PIA rain estimates for ARMAR / TOGA-COARE profile, assuming PIA = 3.9 ± 0.5 dB

Figure 8c: Radar+ radiometer rain estimates for ARMAR / TOGA-COARE profile, assuming $T_b = 254.3° K$

Figure 8d: Radar+ radiometer rain estimates for ARMAR / TOGA-COARE profile, if $T_b = 250° K$

Figure 8e: Radar+ radiometer rain estimates for ARMAR / TOGA-COARE profile, if $T_b = 260° K$

Figure 1

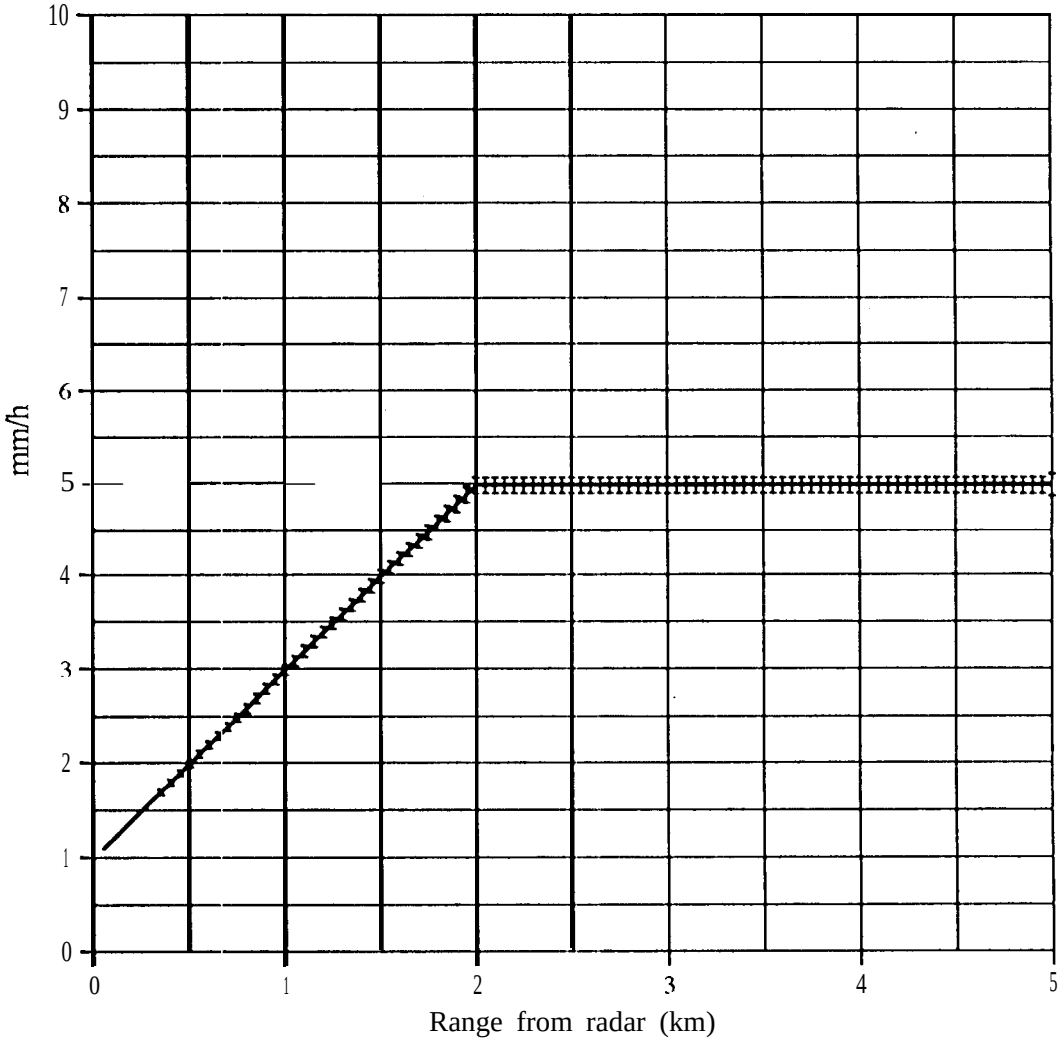

Figure 2a

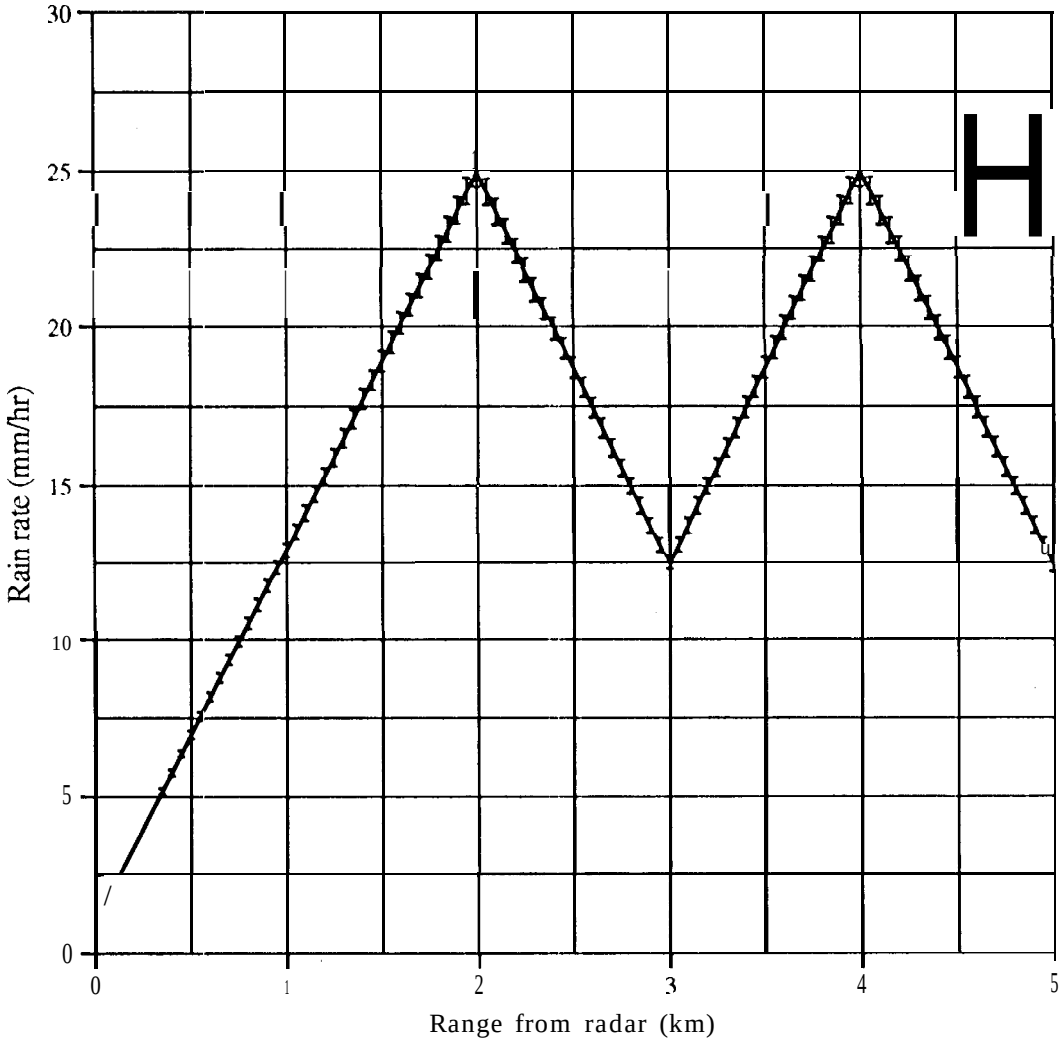

Figure 2b

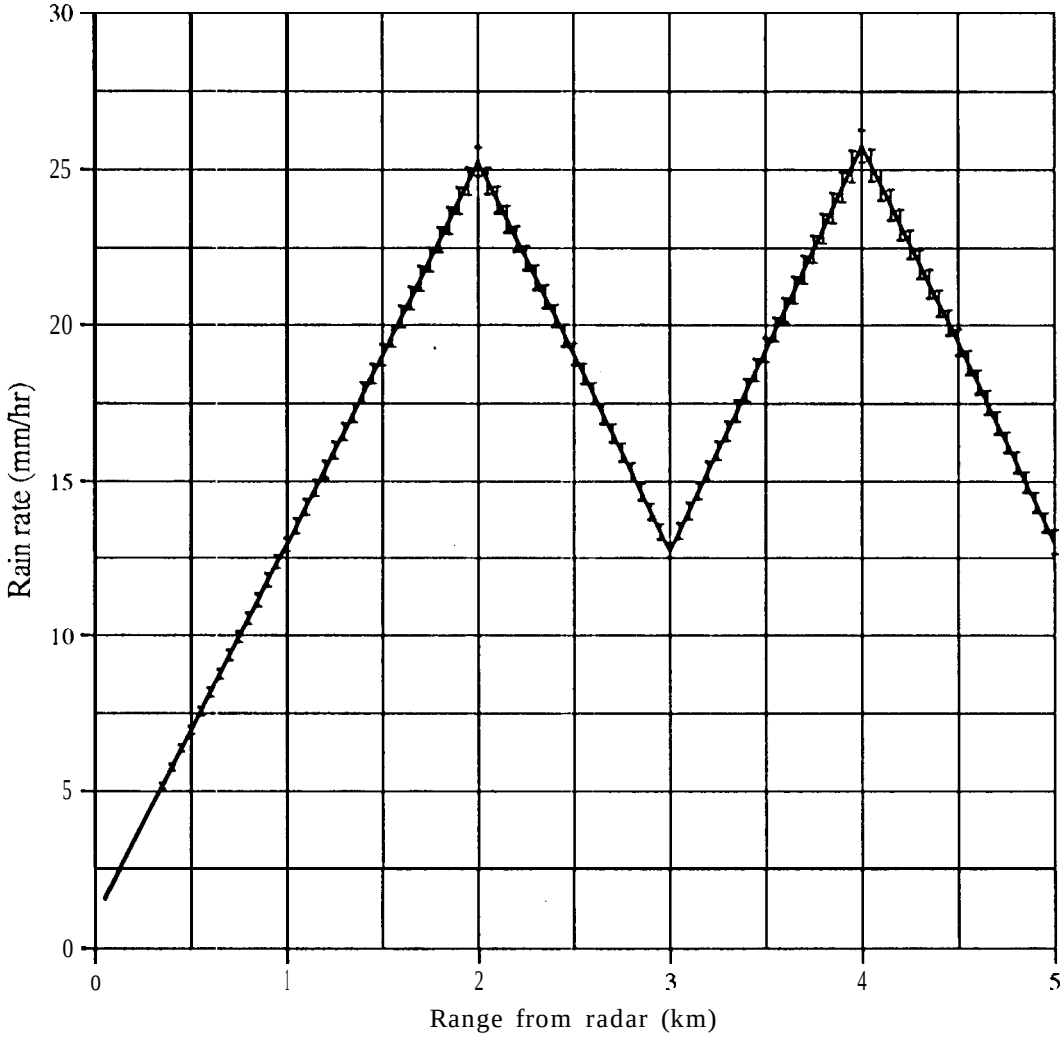

Figure 2c

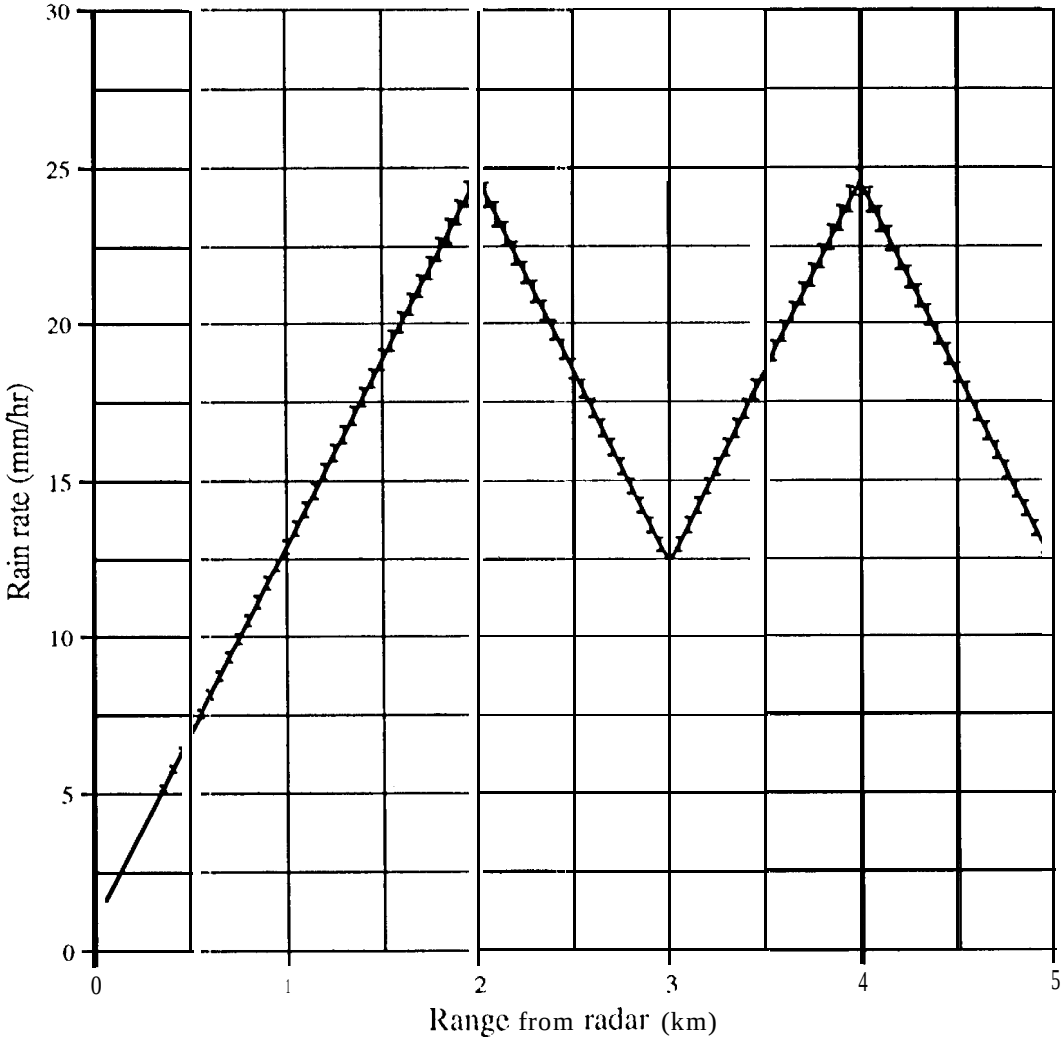

Figure 3a

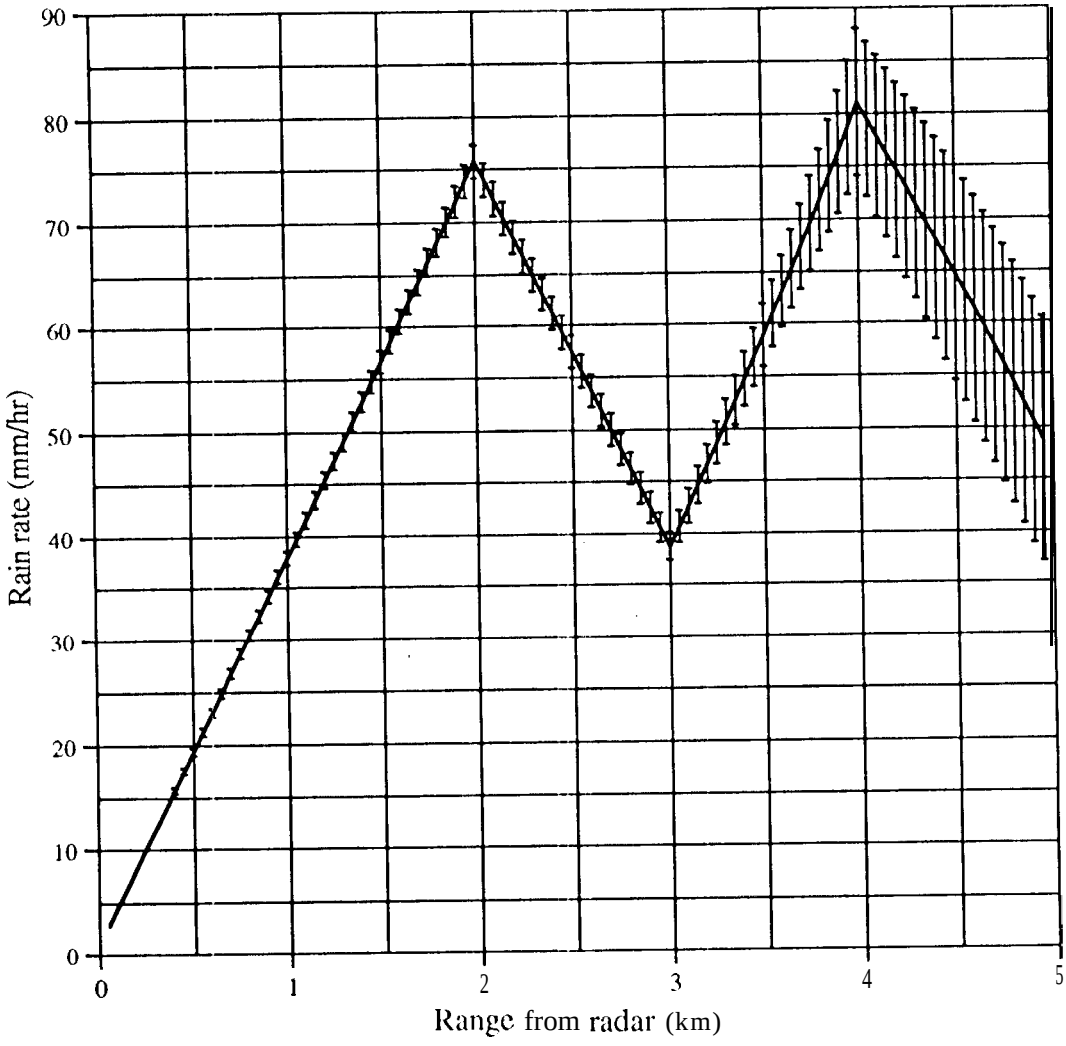
90
80
70
60
50
40
30
20
10
0
Rain rate (mm/hr)
0
1
2
3
4
5
Range from radar (km)

Figure 3b

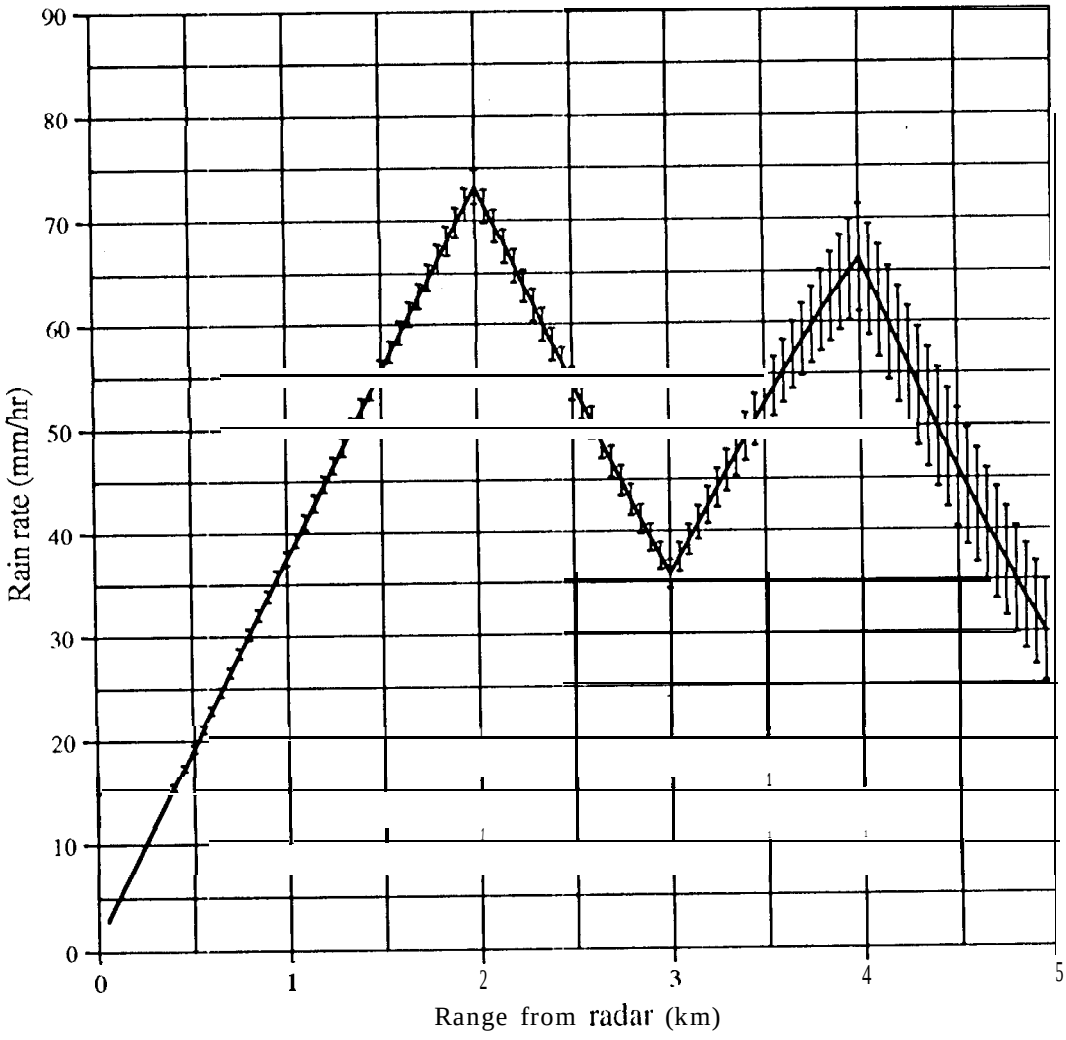
90
80
70
60
50
40
30
20
10
0
Rain rate (mm/hr)
0
1
2
3
4
5
Range from radar (km)

Figure 4a

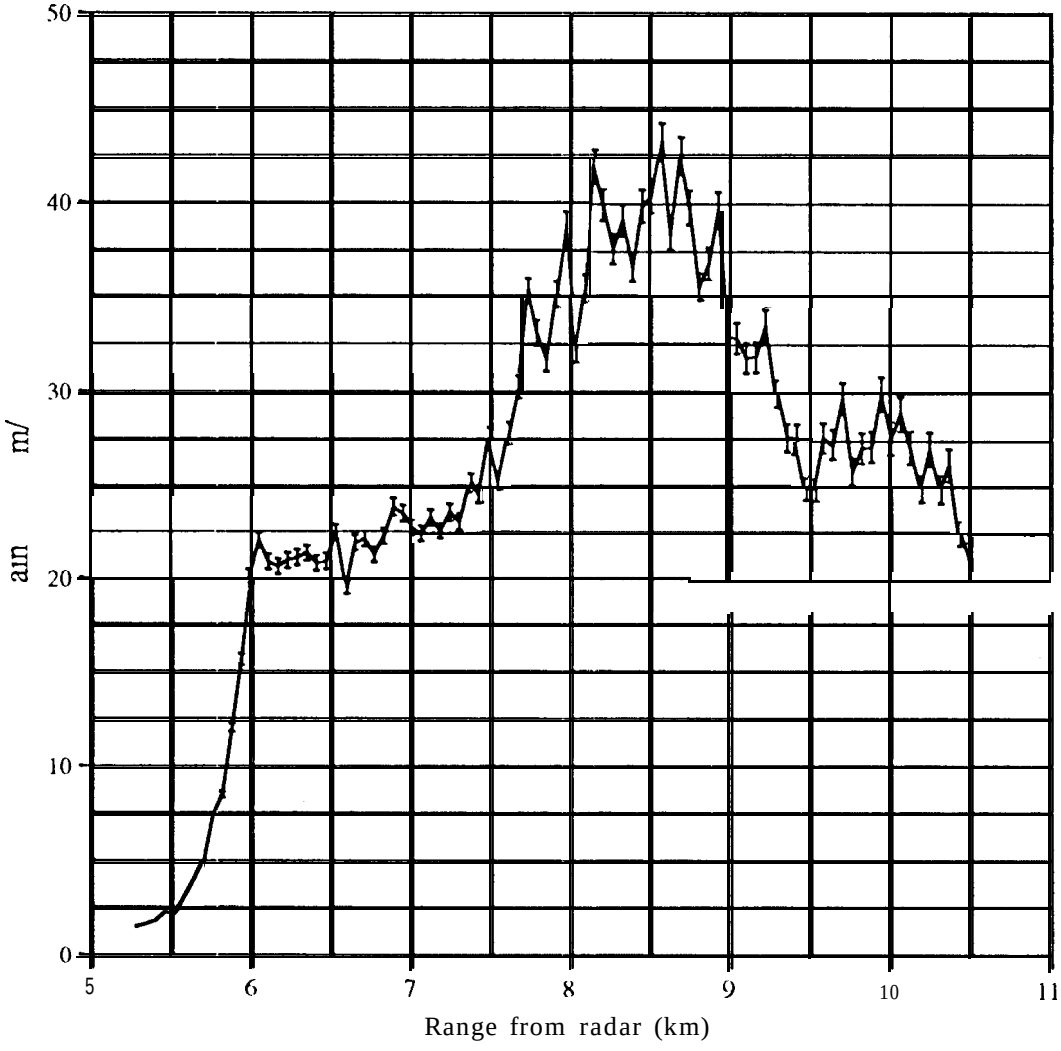

Figure 4b

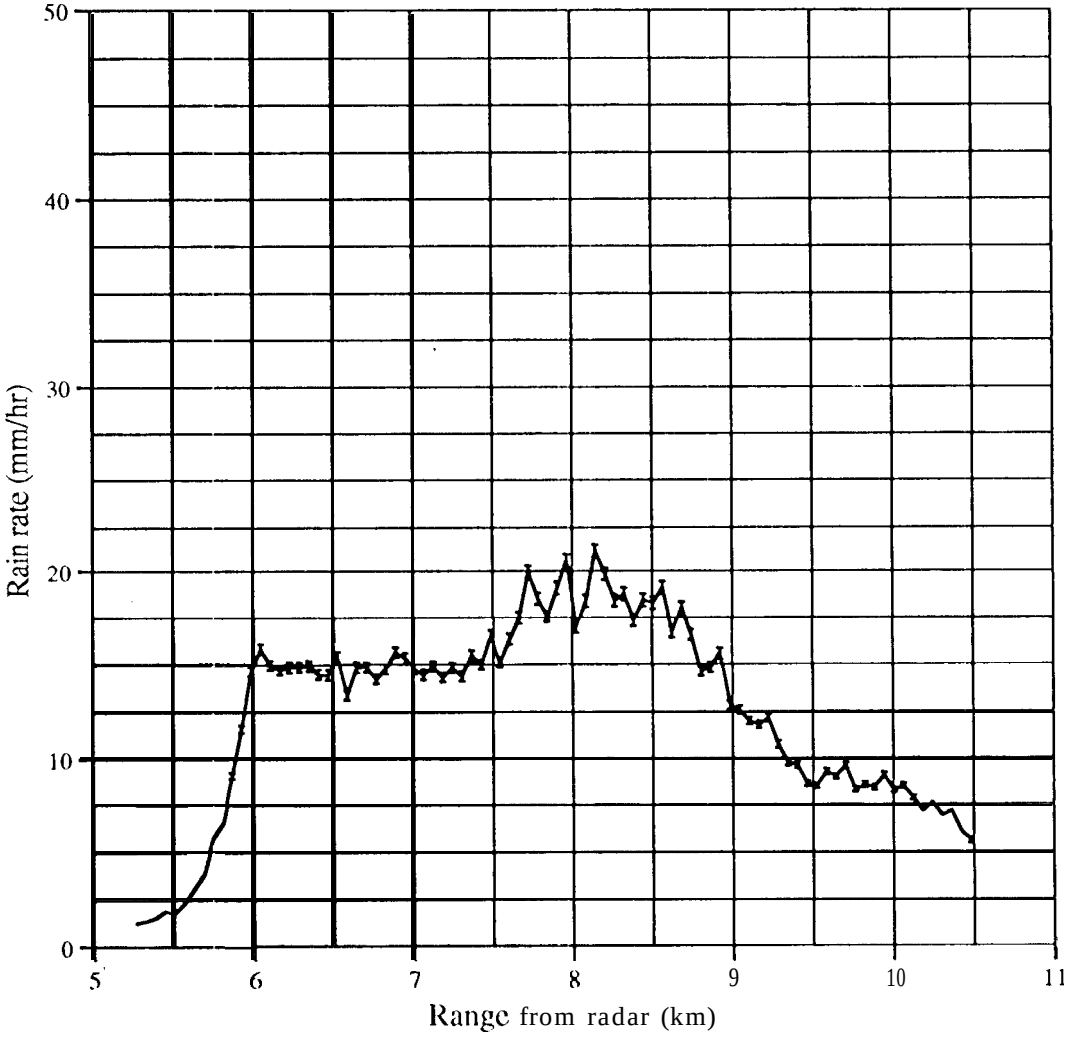

Figure 4C

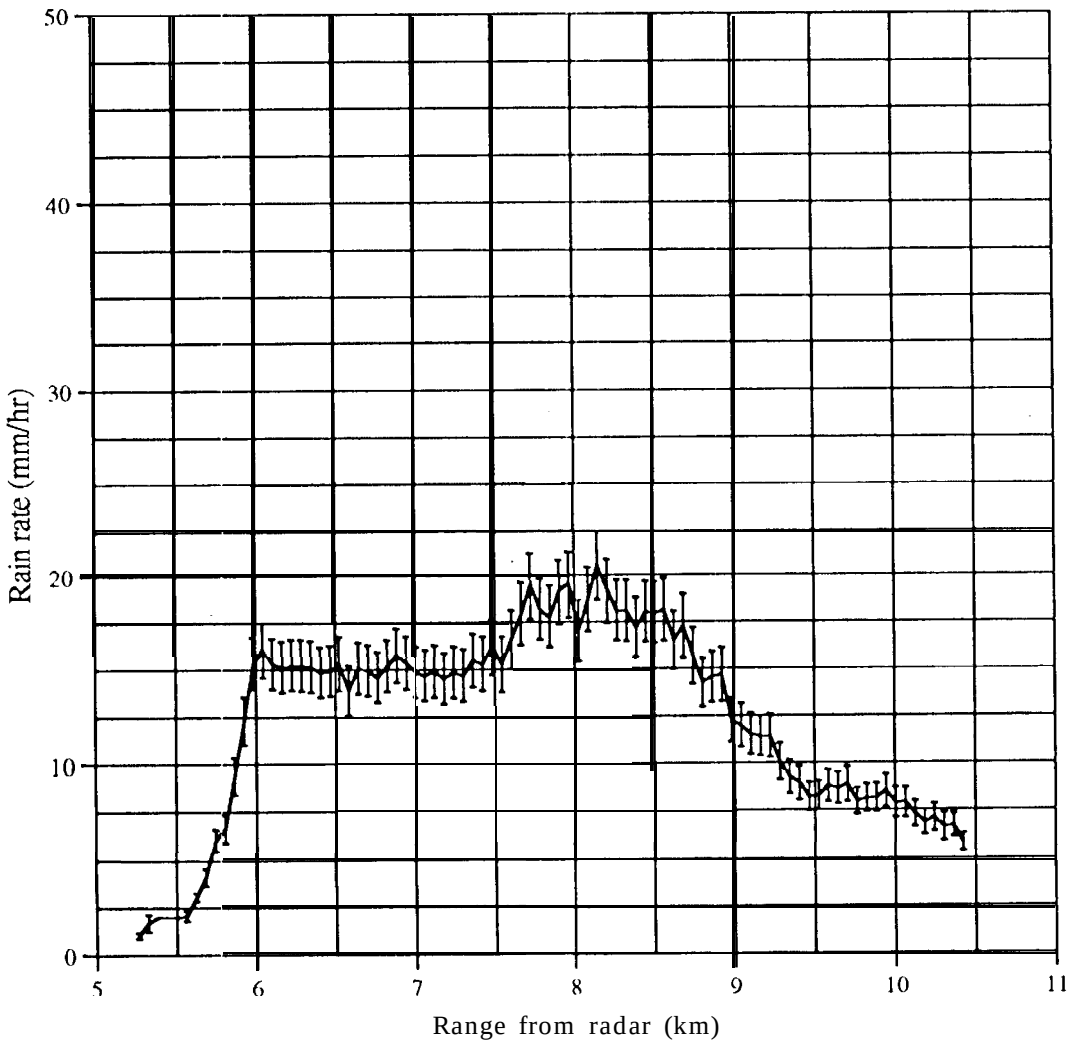

Figure 5

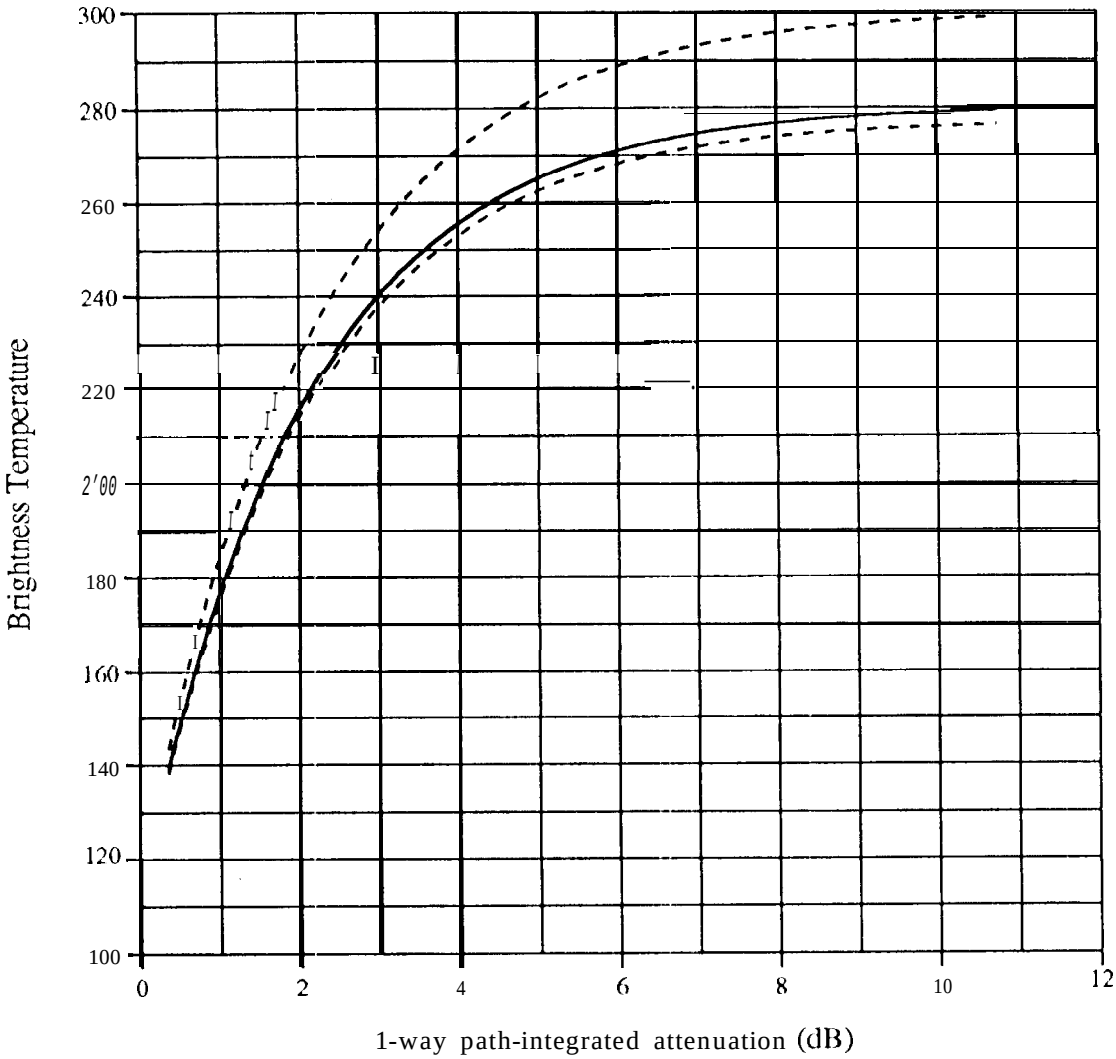
300
280
260
240
220
2'00
180
160
140
120
100
0
2
4
6
8
10
12
Brightness Temperature
1-way path-integrated attenuation (dB)

Figure 6a

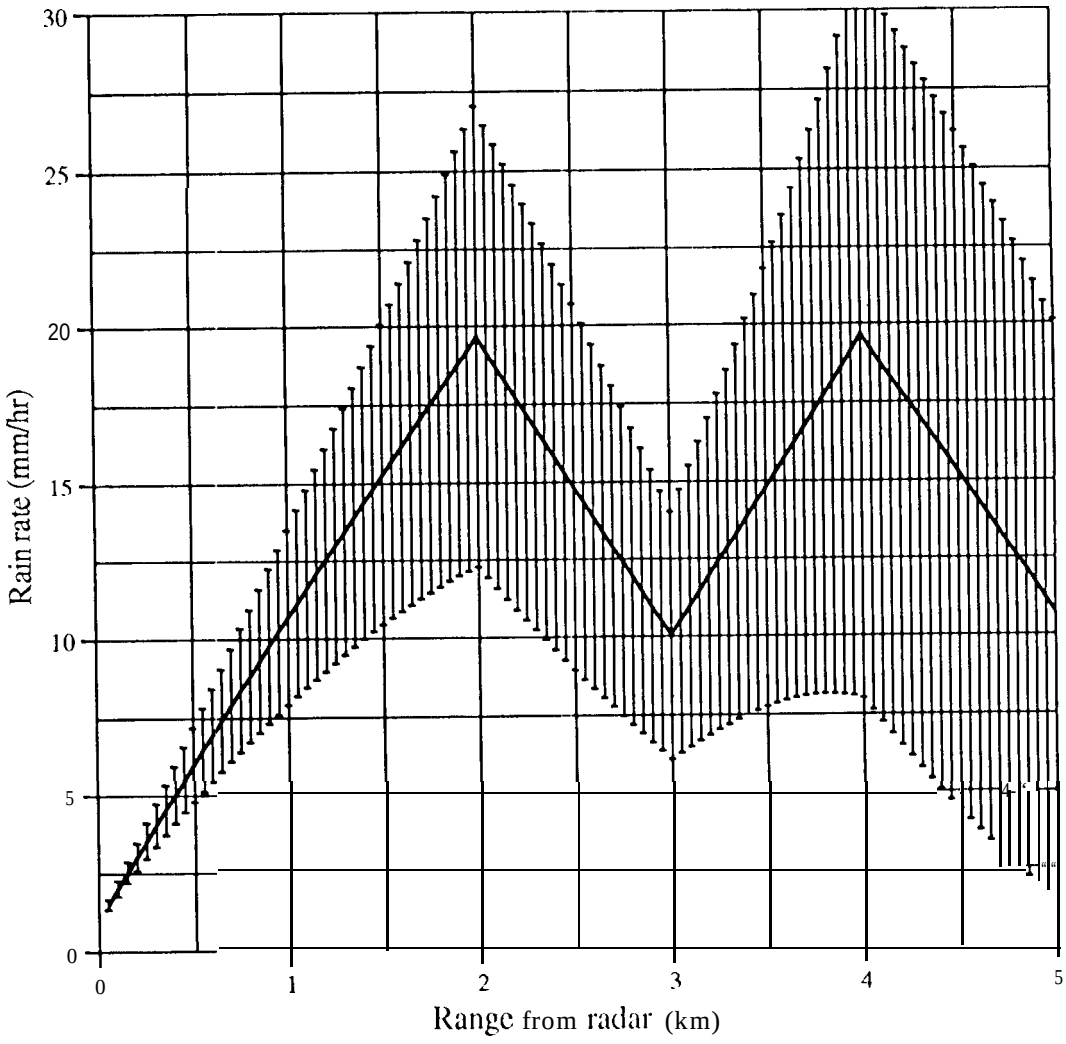

Figure 6b

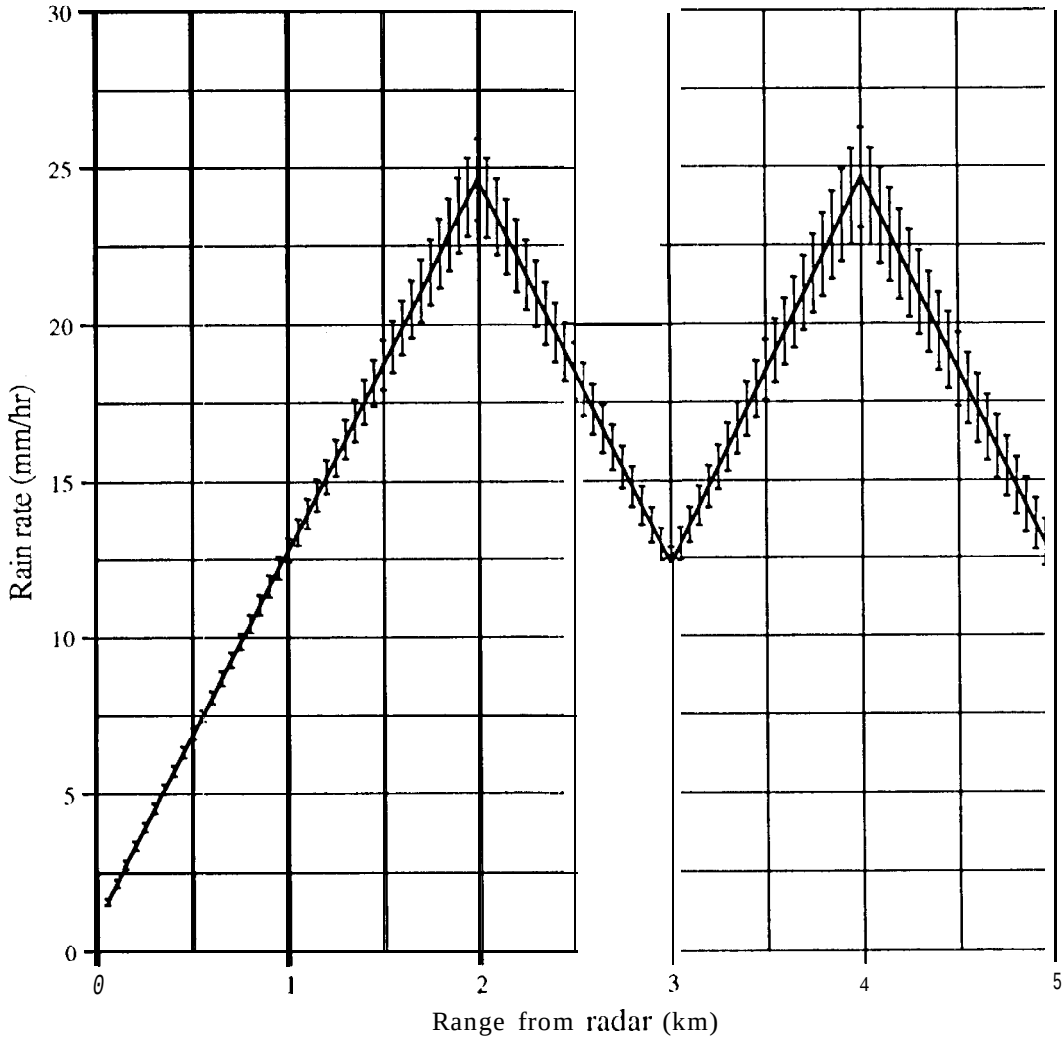

Figure 6c

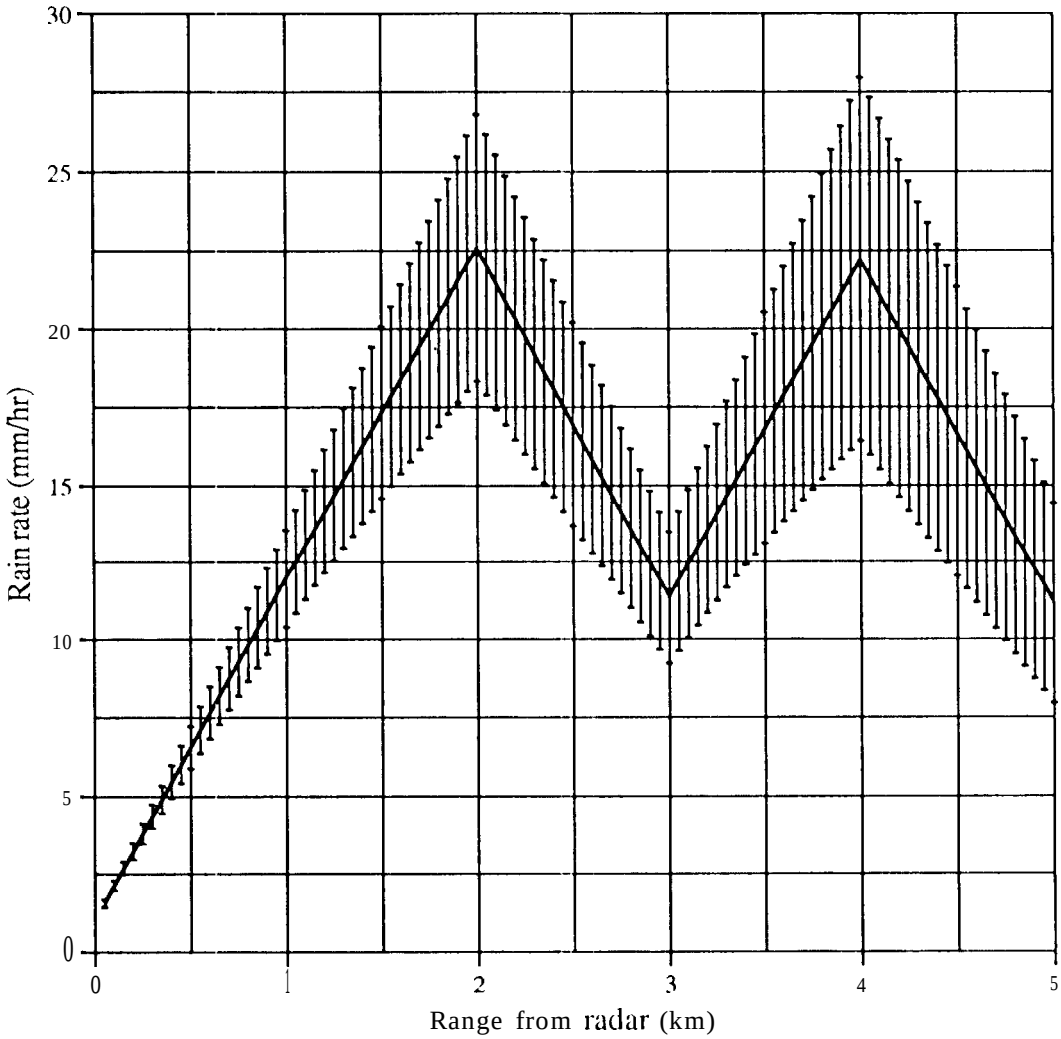

Figure 6d

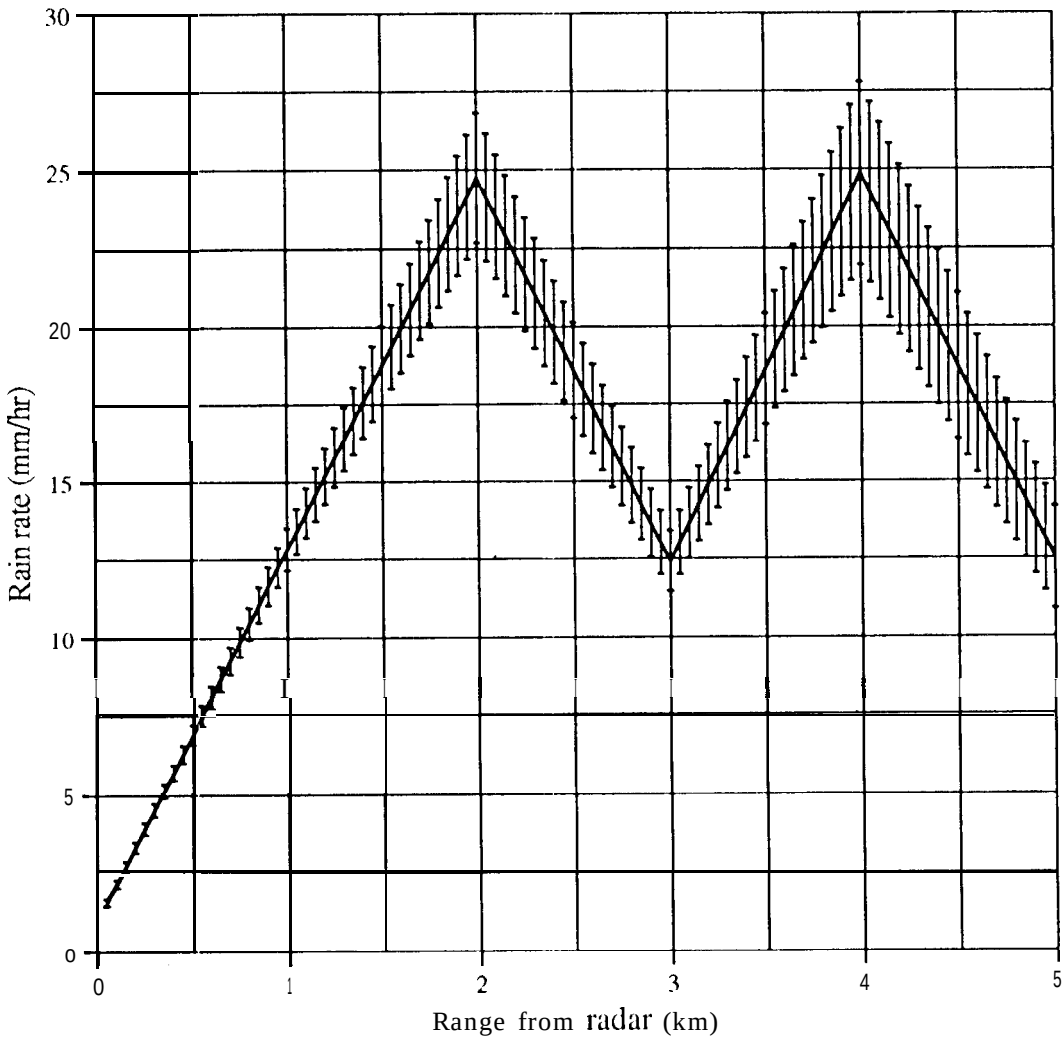

Figure 7a

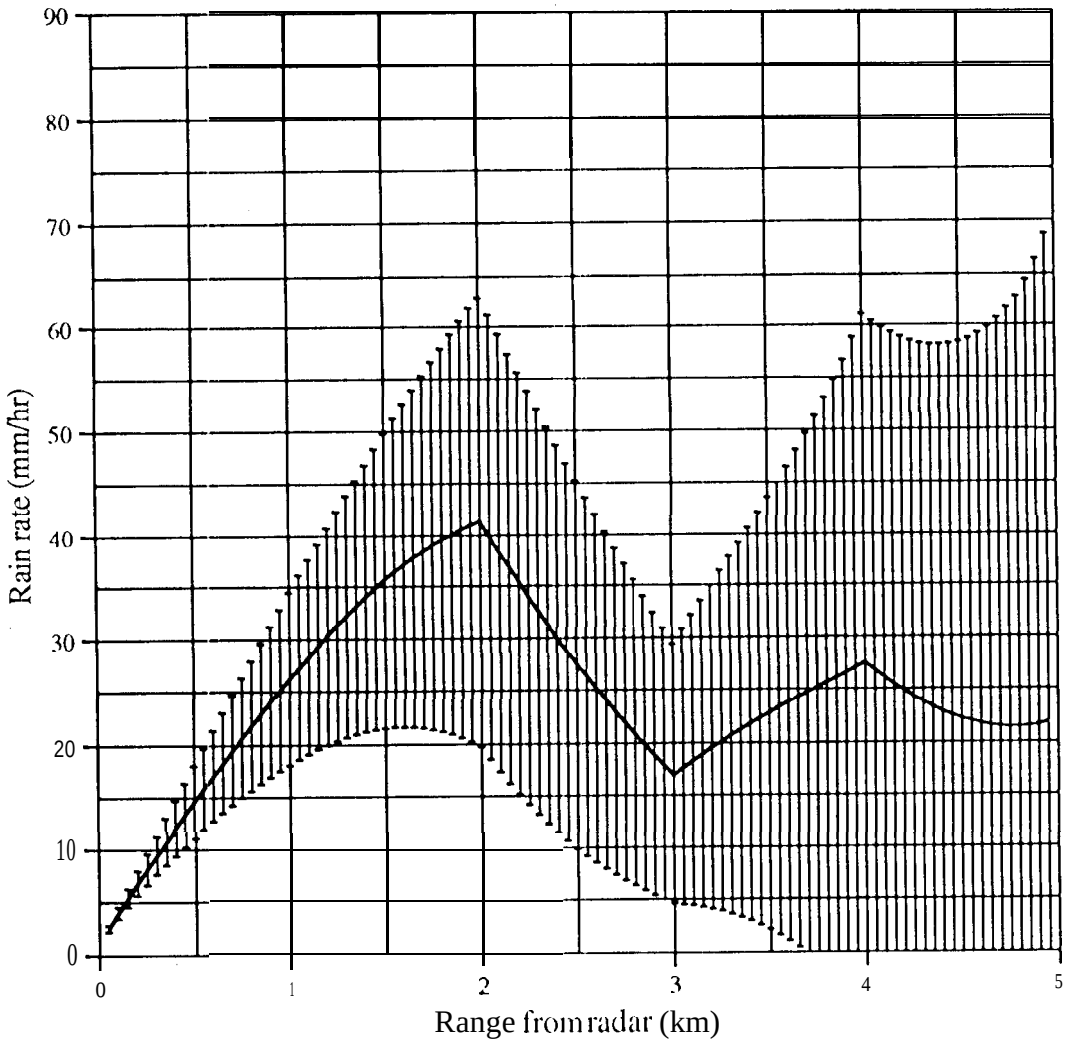
90
80
70
60
50
40
30
20
10
0
Rain rate (mm/hr)
0
1
2
3
4
5
Range from radar (km)

Figure 7b

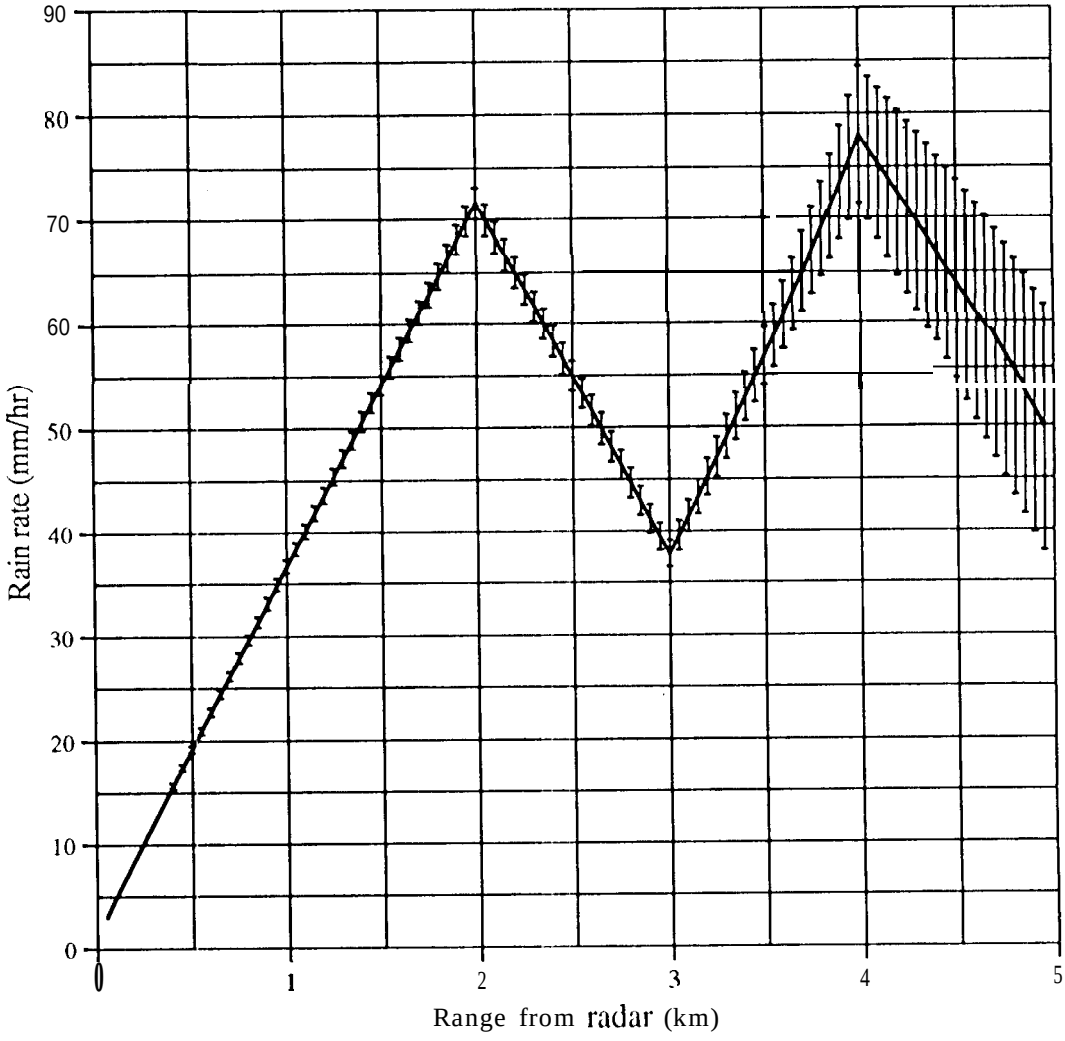
90
80
70
60
50
40
30
20
10
0
Rain rate (mm/hr)
0
1
2
3
4
5
Range from radar (km)

Figure 7c

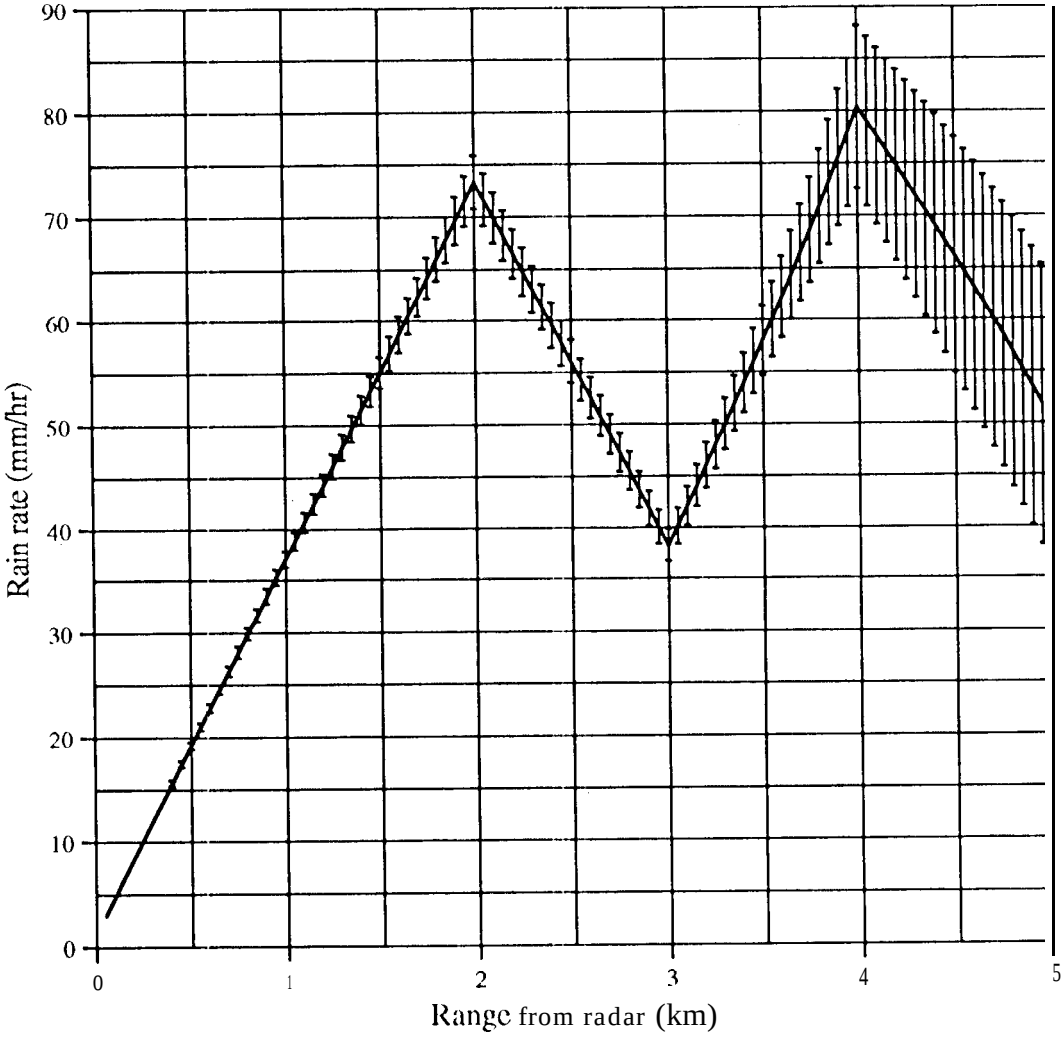
90
80
70
60
50
40
30
20
10
0
Rain rate (mm/hr)
0
1
2
3
4
5
Range from radar (km)

Figure 7d

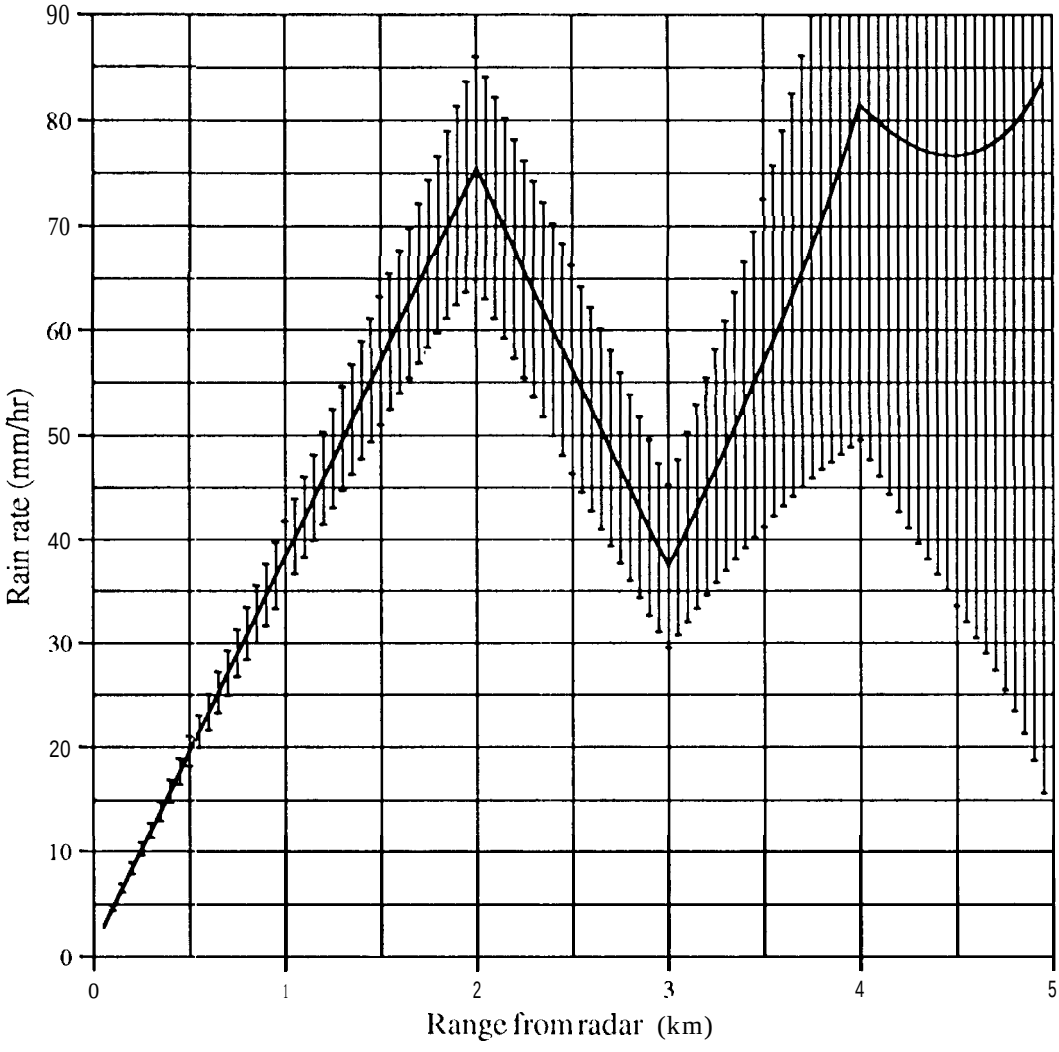
90
80
70
60
50
40
30
20
10
0
Rain rate (mm/hr)
0
1
2
3
4
5
Range from radar (km)

Figure 8a

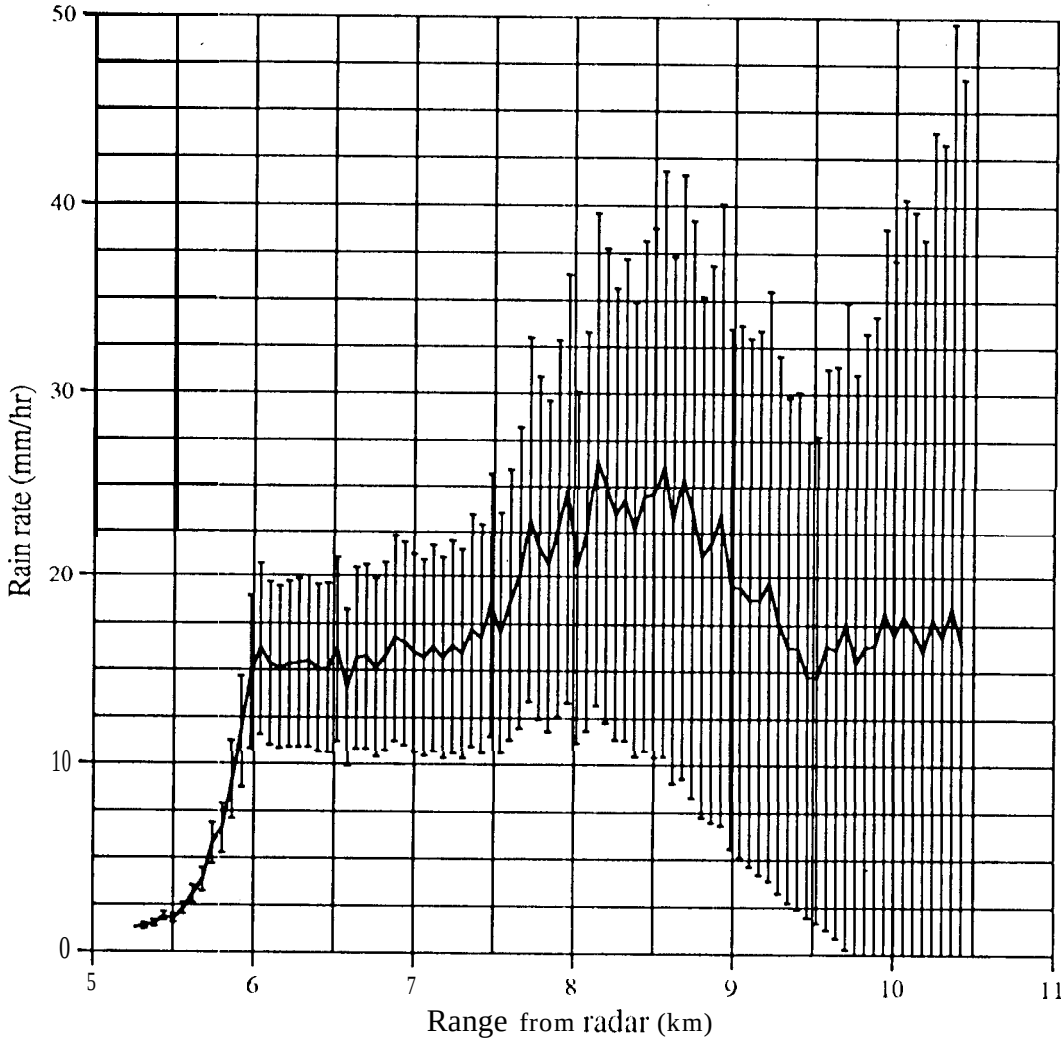

Figure 8b

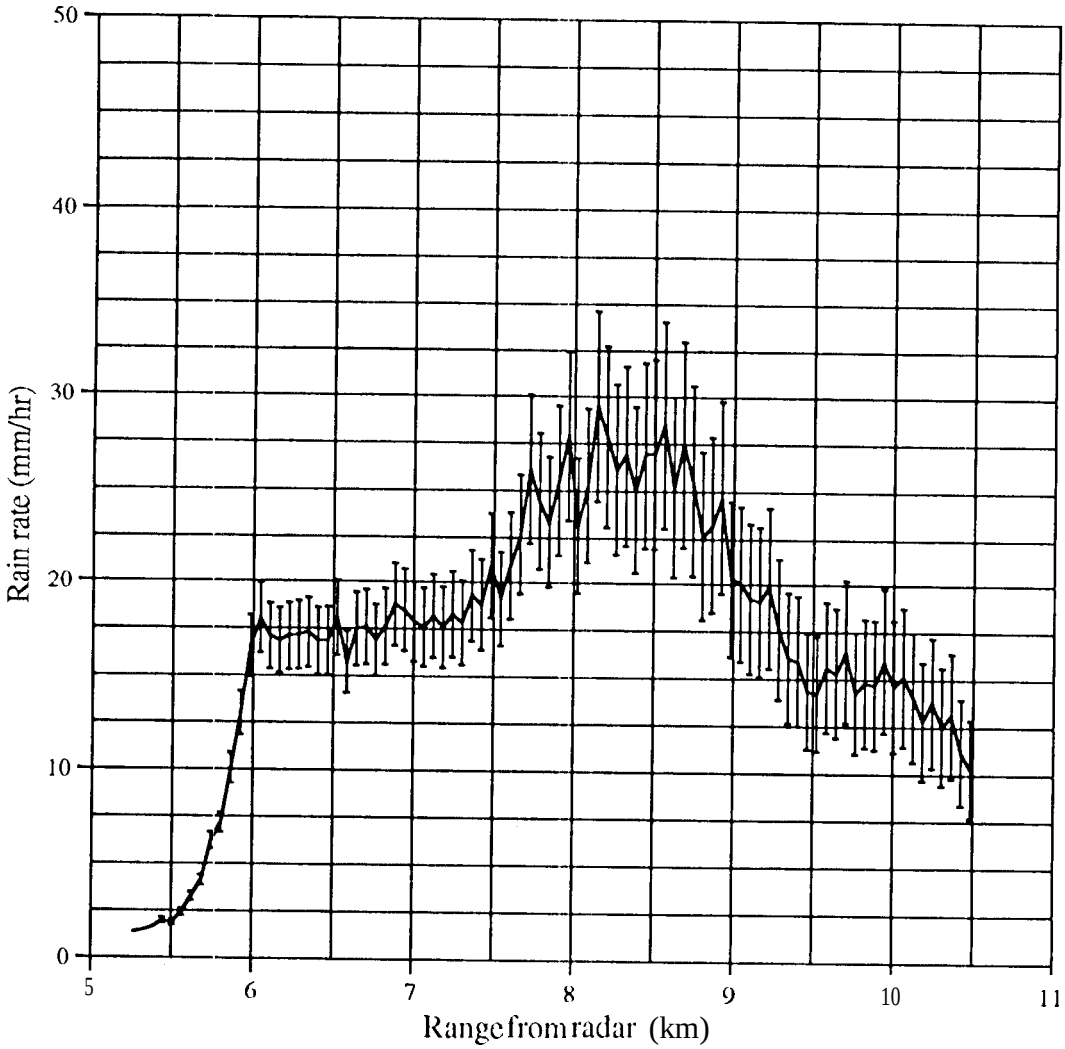

Figure 8c

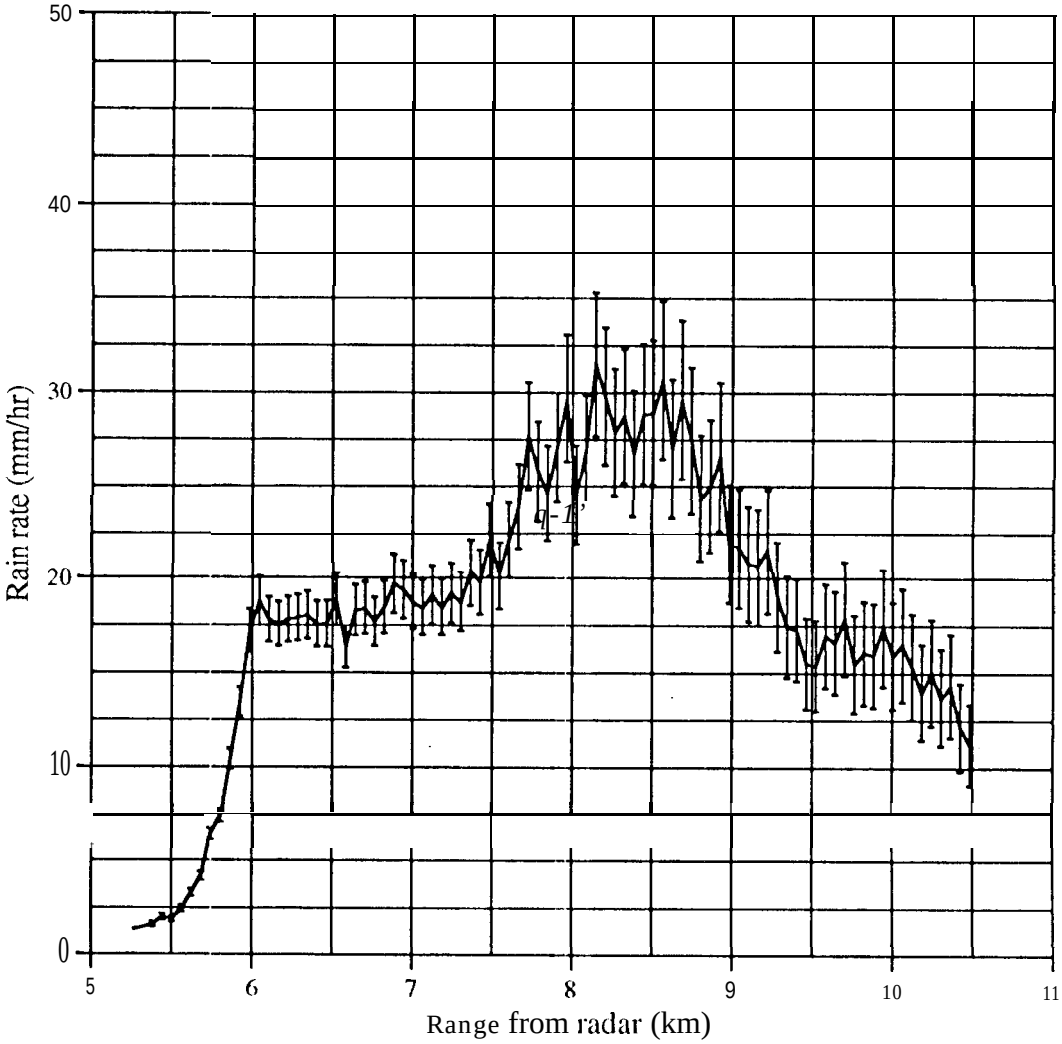
50
40
30
20
10
0
Rain rate (mm/hr)
q-1'
5
6
7
8
9
10
11
Range from radar (km)

Figure 8d

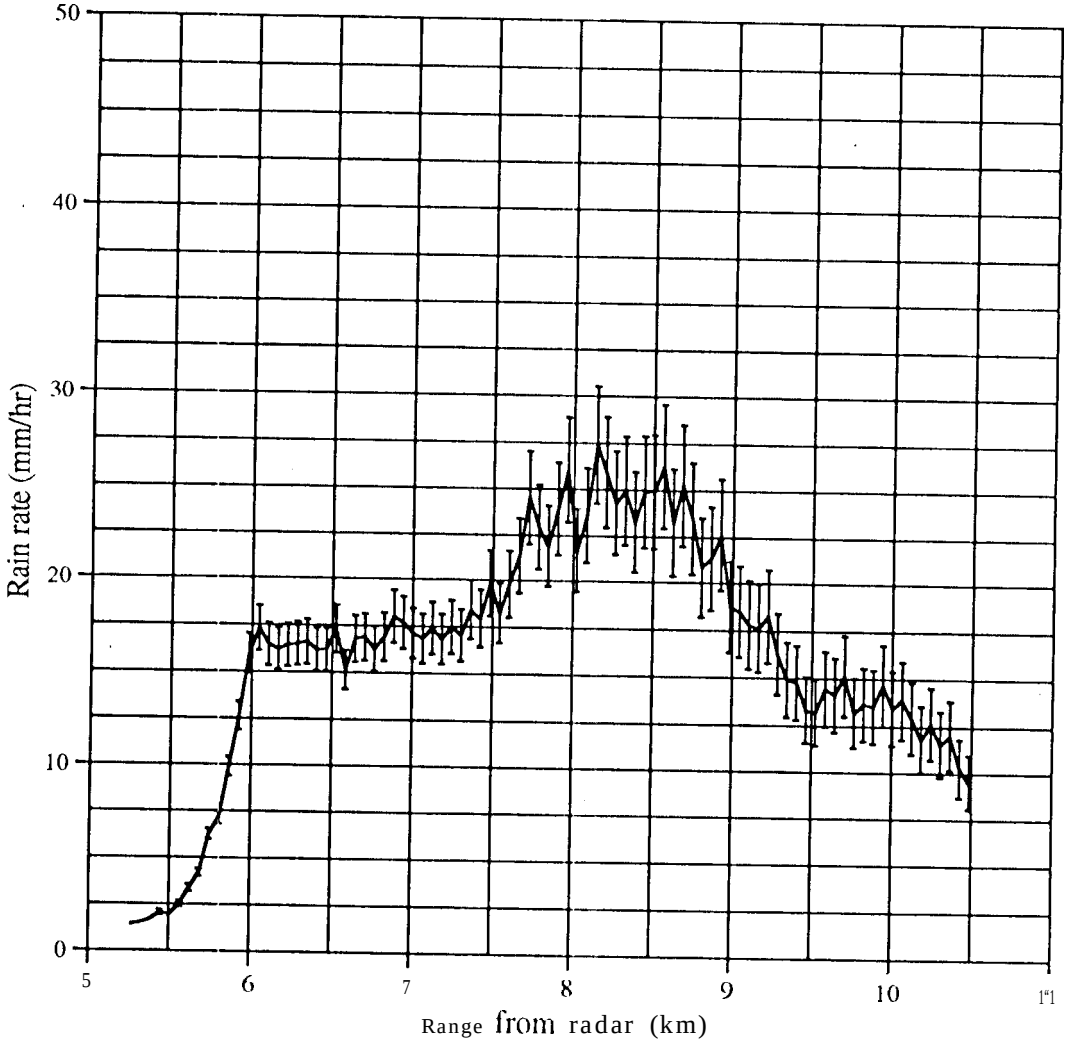

Figure Se